LASER INTERFEROMETER GRAVITATIONAL WAVE OBSERVATORY
- LIGO -
CALIFORNIA INSTITUTE OF TECHNOLOGY
MASSACHUSETTS INSTITUTE OF TECHNOLOGY

Document Type **LIGO-T970144-00 - D** 8/12/97

Input Optics
Preliminary Design

Rana Adhikari, Tom Delker, David Reitze, Qi-Ze Shu, David Tanner, Sanichiro Yoshida

Distribution of this document:

IOO Design Review Board

This is an internal working note
of the LIGO Project.

California Institute of Technology
LIGO Project - MS 51-33
Pasadena CA 91125
Phone (818) 395-2129
Fax (818) 304-9834
E-mail: info@ligo.caltech.edu

Massachusetts Institute of Technology
LIGO Project - MS 20B-145
Cambridge, MA 01239
Phone (617) 253-4824
Fax (617) 253-7014
E-mail: info@ligo.mit.edu

WWW: http://www.ligo.caltech.edu/

TABLE OF CONTENTS

1 INTRODUCTION

1.1. Purpose

This document along with supporting analysis documents presents the current design status for the LIGO Input Optics. The design information in this document supersede that presented in the IOO Conceptual Design and is intended to present a detailed preliminary design for the LIGO Input Optics Subsystem which conform to the *Input Optics Design Requirements,* LIGO-T960093-00-D. This document is intended for the LIGO Detector Team.

1.2. Scope

This document details the current status of the Input Optics design effort. The IOO provides for the conditioning of the laser light after the PSL and before the IFO input, and for the disposition of the IFO reflected light to the LSC and ASC subsystems. It includes RF phase modulation of the light for the generation of resonant and non-resonant sidebands; mode-matching, lock acquisition and operation of the mode cleaner; mode matching of the light to the IFO; beam steering into the IFO; and diagnostic beam pick-offs for the LSC/ASC subsystems.

1.2.1. IOO Subsystems

The Input / Output (IOO) subsystem layout consists of the following units, schematically shown in Figure 1:

- RF modulation
- Steering and conditioning optics
- Mode cleaner and controls
- IFO mode matching and beam pointing
- IFO signal extraction for ASC
- Signal extraction for PSL intensity control

Figure 1: IOO Subsystem Components

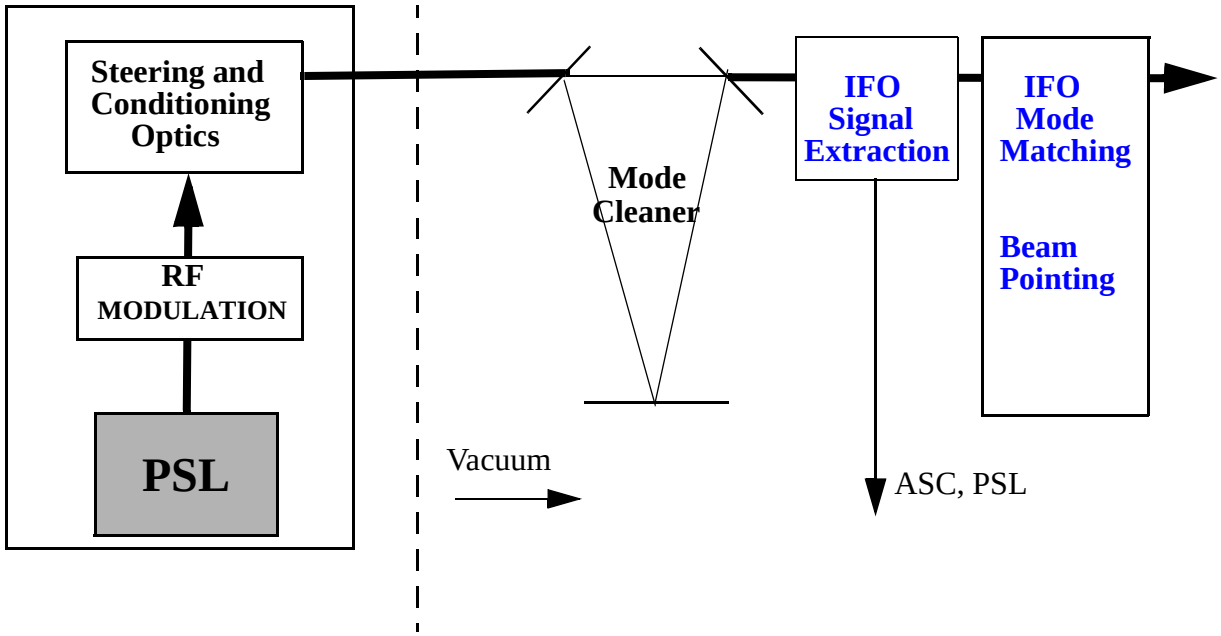

1.2.2. Not in the IOO

The IOO specifically does not include the RF oscillator or suspension designs, baffling of scattered light in the HAMs, the Output Optics, RF photodiodes for PSL or LSC/ASC diagnostic signals.

1.3. Document Organization

1.3.1. Definitions

- TEM_{00} Gaussian beam: A beam of electromagnetic radiation, in which the transverse electric field varies as $E = E_0 e^{-r^2/w^2}$, where w is the beam spot size and E_0 is the electric field strength at r=0.
- Spot size: The characteristic size for Gaussian laser beams, defined as the distance (radius) at which the electric field drops to $1/e$ times the maximum value, E_0 (at $r = 0$).
- Modulation index Γ: The application of RF sidebands using an EOM results in a output field $E_{mod} = E_{in} e^{-i\omega t - i\Gamma\cos\Omega t}$ where ω and Ω are the carrier and modulation frequencies and E_{in} is the input field amplitude.

1.3.2. Acronyms

AM	Amplitude Modulation
ASC	Alignment Sensing / Control (detector subsystem)
BS	Beamsplitter (optical component)
CDS	Control and Data System (detector subsystem)
CMRR	Common Mode Rejection Ratio
COC	Core Optics Components (detector subsystem)
COS	Core Optics Support (detector subsystem)
DC	Direct Current (steady state - low frequency)
EOM	Electro-Optic Modulator (optical hardware)
ETM	End Test Mass (optical component)
FI	Faraday Isolator (optical component)
GW	Gravitational Wave
HAM	Horizontal Access Module
HWP	Half-Wave Plate (optical hardware)
IFO	LIGO Interferometer
IOO	Input Optics (detector subsystem, formerly named Input / Output Optics)
ITM	Input Test Mass (optical component)
LHAM	Horizontal Access Module at Louisiana Site
LIGO	Laser Interferometer Gravitational-Wave Observatory
LSC	Length Sensing / Control (detector subsystem)
LOS	Large Optic Suspension
LVEA	Laser and Vacuum Equipment Area (of the LIGO observatories)
MIT	Massachusetts Institute of Technology
MMT	IFO Mode Matching Telescope
MZ	Mach-Zender Interferometer
Nd:YAG	Neodymium doped Yttrium Aluminum Garnet (laser gain medium)
PDH	Pound-Drever-Hall (reflection locking technique)
PM	Phase Modulation
PSL	Pre-Stabilized Laser (detector subsystem)
PZT	Piezo-electric Transducer (mechanical hardware)
RC	Radius of Curvature of a Reflective Mirror
RF	Radio Frequency
RM	Recycling Mirror
SEI	Seismic Isolation
SOS	Small Optic Suspension
TBD	To Be Determined
TGG	Terbium-Gallium-Garnet (optical material used in Faraday Isolators)
TFP	Thin Film Polarizer (optical hardware)
WFS	Wave Front Sensors
WHAM	Horizontal Access Module at Washington Site

1.3.3. Relevant Documents

1.3.3.1 LIGO Documents

Input Optics Design Requirements Document, J. Camp, D. Reitze, and D. Tanner, *LIGO-T960093-00-D*
Input Optics Conceptual Design, J. Camp, D. Reitze, and D. Tanner, *LIGO-T960170-00-D*
Absorption in the Core Optics and LIGO Sensitivity, LIGO-T970xxx-00-D
ASC Initial Alignment, K. Mason and M. Zucker, *LIGO-T970151-00-D*
Alignment Sensing/Control Design Requirement Document, P. Fritschel, *LIGO-T952007-03-I*
Alignment Sensing/Control Preliminary Design, P. Fritschel, G. Gonzalez, D. Sigg, M. Zucker, *LIGO-T970060-00-D*
Detector Subsystems Requirements, D. Shoemaker, *LIGO-E960112-05-D*
Design Considerations for LIGO Mode-Matching Telescopes, T. Delker, R. Adhikari, S Yoshida, and D. Reitze, *LIGO-T970143-00-D*
Do wiggle effects depend on mode cleaner length, A. Abramovici, *LIGO Technical Note #20* (1988).
Effects of Stray Magnetic Fields Generated by Faraday Isolators on Suspended Optical Components, S. Yoshida, R. Adhikari, and D. Reitze, *LIGO-T970149-00-D*
Estimation of Special Optical Properties of a Triangular Mode Cleaner, F.J. Raab and S.E. Whitcomb, *LIGO Technical Note #108 (1992).*
Frequency Stabilization: Servo Configuration & Subsystem Interface Specification, P. Fritschel, *LIGO-T970088-00-D*
Impact of Non-resonant Sidebands on Length Sensing Signals, J. Camp, *LIGO-T970097-00-D*
(Infrared) Pre-Stabilized Laser (PSL) Conceptual Design, R. Abbott, P. King, R.Savage, S Seel, *LIGO-T970087-00-D*
Initial length precision of LIGO suspended cavities, J. Camp, *LIGO-T960181.*
LIGO cavity lengths and modulation frequencies, D.B. Tanner, *LIGO-T-970xxx-03-D*
MIT Meeting on RF Modulation, Davd Shoemaker, LIGO-T970155-00-D
Modal Model Update 4: Mode-Matching, D. Sigg, *LIGO-T960116-00-D*
Modal Model Update 6: Mode Cleaner, D. Sigg, *LIGO-T960118-00-D*
Mode Cleaner Noise Sources, J. Camp, *LIGO-T960165-00-D*
Proposed initial detector MC and RC baseline lengths, M. Zucker and P. Fritschel, *LIGO-T960122-00-I.*
Recycling cavity and mode cleaner baseline dimensions, D. Coyne, *LIGO-T970068-00-D*
Seismic Isolation Design Requirements, Fred Raab, *LIGO T960065-03-D*
Small Optics Suspensions Final Design, S. Kawamura, *LIGO-T970135-02-D*

1.3.3.2 Non-LIGO Documents

Heating by Optical Absorption and the Performance of Gravitational Wave Detectors, W.Winkler, K. Danzmann, A. Ruediger, and R. Schilling, Phys Rev A, 44, 7022.
Optical mode cleaner with suspended mirrors, A. Araya, N. Mio, K. Tsubono, K. Suehiro, S. Telada, M. Ohashi, and M. Fujimoto, Appl. Opt. **39**, 1446 (1977).
The response of a Fabry-Perot optical cavity to phase modulation sidebands for use in electro-optic control systems, K.D. Skelton, and K.A. Strain, Applied Optics Lasers, *in press.*
Alignment of Resonant Optical Cavities, D. Anderson, Appl. Opt. **23**, 2944 (1984).

2 OVERVIEW OF THE DESIGN STATUS

2.1. Design Changes

Since the IOO conceptual design, four major design changes have taken place in the IOO subsystems:

2.1.1. Replacement of the baseline RF modulation method

In the IOO Conceptual Design, we proposed a split-path, Mach-Zender interferometer in which the synthesis of the resonant and non-resonant sidebands would occur on different optical paths, thus avoiding the generation of intermodulation cross-products. Our initial design was motivated by concerns of possible in-band noise at the GW dark port caused by mixing of resonant and non-resonant sidebands. Although some pathways have been identified (c.f., *Impact of Non-resonant Sidebands on Length Sensing Signals*,LIGO-T970097-00-D*; MIT Meeting on RF Modulation*, LIGO-T970155-00-D*)* none have definitively shown to have an effect. While not all pathways can be identified a priori, we feel that the 'cost' of implementing the MZ RF modulation (development of length and alignment controls) weighed against the simpler alternative scheme, namely serial modulation with two EOMs, was high in light of the fact that analysis had failed to identify any specific problem with intermodulation cross-products.

A simple, dual EOM serial modulation method will be used to apply resonant and non-resonant sidebands.

2.1.2. Use of a three element reflective telescope

The IOO Conceptual Design proposed a two-element reflective mode-matching telescope for mode-matching into the COC. For allowing more flexibility in mode-matching to the COC (for example, to compensate for variations in COC and IOO components due to polishing error or thermal deformations), we have refined the design to a three element reflective mirror telescope. This design allows for optimization of mode-matched power by having independent adjustment of two degrees of freedom (waist size and position or, alternatively, wavefront radius of curvature and beam divergence angle).

A three element telescope consisting of spherical reflective optics will be used for mode-matching into the COC.

2.1.3. Use of a third frequency for locking the mode cleaner

In the conceptual design, the mode cleaner was to be locked by the resonant sideband frequency, using a deliberate detuning of the resonant sideband frequency from resonance frequency, so that some of the sideband power would be reflected and give a signal proportional to the offset of the carrier from mode cleaner resonance. (The modulation depth of the nonresonant sideband is insufficient for mode cleaner lock.) Because the detuning might lead to additional phase and amplitude noise in the resonant sideband, a third EOM will be used to generate a sideband that is non resonant in the mode cleaner for locking the mode cleaner.

A third EOM serial modulation method will be used to generate sidebands for mode-cleaner locking.

2.1.4. Elimination of first Faraday isolator

The conceptual design contained a Faraday isolator as the first optical element of the input optics. This duplicates the function of a Faraday isolator in the PSL subsystem[1] (protection of the laser oscillator from optical feedback). It has been removed from the preliminary design as redundant.

There is no Faraday isolator at the front end of the input optics.

2.2. Areas which need more work

There are a few areas which we feel have not yet been given sufficient attention by the IOO group:

- Mode Cleaner Length Controls - We have not yet come up with a complete servo design for locking the mode cleaner to the levels specified in the *IOO Design Requirements Document*. We expended significant manpower resources since the conceptual design on the fabrication of a prototype MZ RF modulation scheme. Since the MZ has been abandoned as the baseline design for sideband generation, this will free up the manpower necessary to complete the design and pass it to the CDS group.
- Measurement of Mode-Matching to the COC - The proposed MMT design will allow us to vary the spatial mode parameters of the beam sufficiently to accommodate expected variations in optical components (see Section 8.1). Nonetheless, our design requires some motion of the MMT optics in the vacuum to be able to determine the higher order mode content and necessary adjustment. We propose to develop a design based on using ‘doughnut’ (circularly split) photodiodes (*Modal Model Update 6: Mode-Matching, LIGO-T970116-00-D*) to detect small changes in coupled power caused by dithering of MMT mirror 1 and 2. This circumvents the need for in-vacuum automated mechanical motion of the SOS suspensions. Prototyping and testing of this system has not yet taken place.
- Measurements of High Power Effects in IOO optics - In as far as possible, we have made estimates of the effects of high power beam propagation through transmissive optics in the IOO chain. Nonetheless, no hard data has been obtained. We feel it is imperative to measure these effects and will conduct a testing program (see Section 10) before the IOO Final Design Review to identify potential problems.

1. (I*nfrared) Pre-Stabilized Laser (PSL) Conceptual Design*, R. Abbott, P. King, R.Savage, S Seel, *LIGO-T970087-00-D*

3 SUBSYSTEM INTERFACES

3.1. PSL

3.1.1. Optical

3.1.1.1 Main Beam

The output beam from the PSL will be delivered to IOO at (60.5 in ±0.25in,12.5 in ±0.25in) in the optical table local coordinate system defined in Figure 2. The spot size at the beam waist, w_0, of the PSL output beam shall be 0.5 mm ±0.1 mm. The PSL output beam waist location shall be within 5.0 cm of the PSL output beam location.

3.1.1.2 PSL Intensity Pick-off

The intensity stabilization beams for the PSL will be delivered to the PSL photodiode located (**TBD ISC**) on the ISC tables located adjacent to HAM 1 (4 km IFO) and HAM 7 (2 km IFO). At the IOO/PSL interface location, the spot size of the IOO output beam sample for power stabilization shall be 2.0 mm ±0.2 mm**.** The power of the beam shall be 50 mW (**TBD PSL/IOO**).

3.1.2. Mechanical

The IOO shares an optical table with the PSL (PSL/IOO table).Figure 2 shows the allocation of table area for each subsystem. The optical table itself as well as the physical enclosure surrounding the table (for controlling acoustic noise, air currents, dust, and thermal variations) is the responsibility of the PSL subsystem. IOO is responsible for the positioning of the PSL/IOO table and the vibration isolation of the table from the LVEA floor.

The distance from the PSL/IOO optical table surface to the LVEA floor is 89cm ±1.0 cm

Figure 2: Shared PSL/IOO Optical Table

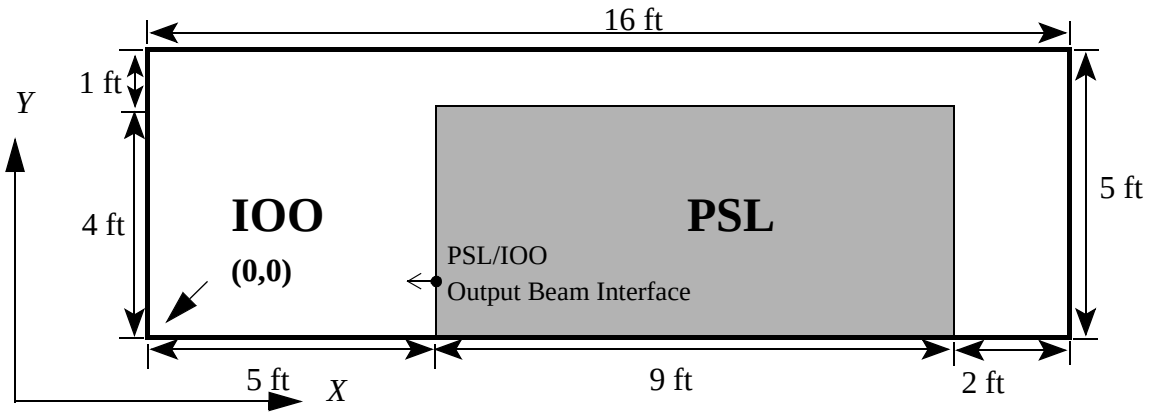

3.2. COC

3.2.1. Optical

3.2.1.1 4 km IFO

The IOO delivers the optical beam to the 4 km RM at (X,Y,Z) = (-4.596 m, 0.212 m, 0.026 m) to within ± 1 mm and $\pm 2.5 x 10^{-7}$ rad in the LIGO Global Coordinate System

3.2.1.2 2 km IFO

The IOO delivers the optical beam to the 2 km RM at (X,Y,Z) = (12.184 m, 9.060 m, 0.043 m) to within ± 1 mm and $\pm 2.5 x 10^{-7}$ rad in the LIGO Global Coordinate System

3.3. ISC

3.3.1. Optical

The IOO delivers diagnostic beams to the ISC subsystems from Faraday Isolators located in WHAM 1 (WA 4 km IFO), in WHAM 7 (WA 2 km IFO), and LHAM 11 (LA 4 km IFO) through access ports (**TBD/ISC)**. These beams will have spot sizes of 2 mm ± 0.1 mm with nominal powers of 300 mW and up to 6 W during lock acquisition of the IFO.

3.3.2. Mechanical

The IOO requires optical levers for positioning of the telescope optics in the HAM chambers. The locations of the optical lever hardware for the MMT are shown in Figure 3 for Table ISC1 (**TBD/ISC)**. In addition, the IOO requires three quadrant photodiodes per IFO to maintain beam centering for the 2 km and 4 km MMT. The location of these diodes is on the ISC tables is **TBD/ISC.**

Figure 3: ISC Table Located Adjacent to HAMs

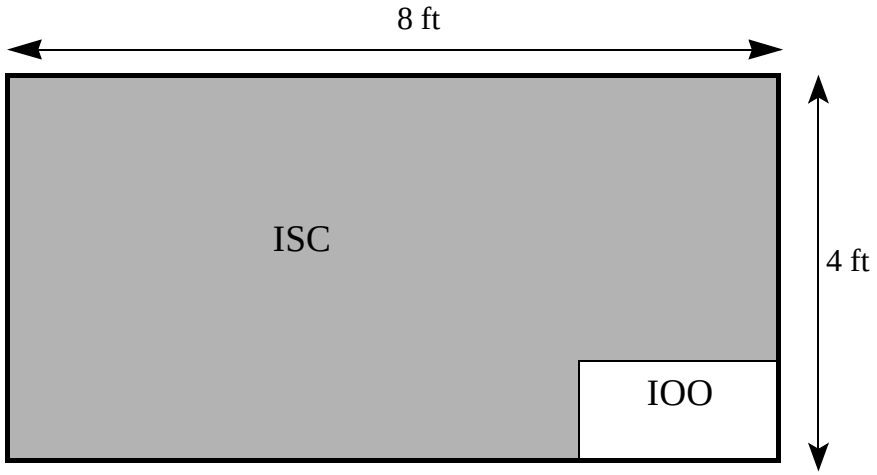

3.3.3. Electrical

The RF modulation signals for the resonant and non-resonant sidebands are supplied to the IOO EOMs from LSC (resonant, Γ=0.47) and ASC (nonresonant; Γ=0.05). IOO will use resonant Mg0:$LiNbO_3$ electro-optic phase modulators (TBD/IOO) with the following characteristics:

- Manufacturer: New Focus
- Model: 4003-DB MgO:$LiNbO_3$ Brewster angle cut modulator.
- Maximum Optical Power: 8 W/mm^2 (**TBD IOO**)
- Modulation Depth $(\Delta\phi)/V$: 0.2 rad/V (depends on frequency; **TBD IOO**)
- Aperture: 2 mm
- Input Impedance: 50 Ω

The signal characteristics are given in Table 1.

Table 1: RF Signals into IOO

Sideband	*Frequency (MHz)*	*Voltage*	*RF Power, RMS (into 50 Ω)*
4 km IFO resonant	24.493	4.7 V pk-pk (Γ=0.47), (**TBD IOO**)	0.25 W (**TBD IOO**)
4 km IFO non-resonant	61.232 (**TBD ASC**)	0.6 V pk-pk (**TBD IOO**)	~1 mW (**TBD IOO**)
2 km IFO resonant	29.486	4.7 V pk-pk (Γ=0.47), (**TBD IOO**)	0.25 W (**TBD IOO**)
2 km IFO non-resonant	68.800 (**TBD ASC**)	0.6 V pk-pk (**TBD IOO**)	~1 mW (**TBD IOO**)

Note: Modulation indices Γ are nominal; the modulation depths for the resonant sidebands are to range from 0-1. The range of modulation depth for the non-resonant sideband of **TBD ISC** will be provided by ISC.

3.4. SEI

3.4.1. Mechanical

The in-vacuum IOO components are located on the seismic isolation stacks located in WHAM 1,2,7,8 and LHAM 11,12.

4 OPTICAL LAYOUT

4.1. Physical Implementation

We assume that the LIGO facilities meet the specifications for vibrational and acoustic noise given in the Civil Construction Facilities *Design Configuration Control Document*, LIGO C960703-0.

4.2. PSL/IOO Table

4.2.1. Position of the Optical Table in the LVEA

The PSL/IOO table will be located at the entrance port to WHAM 1 and WHAM 1 (LIGO global coordinates such that the centerline of the optical table is situated on the centerline of the beam tube to ±0.5 inches. See Figure 4. At Livingston, La, the single optical table will be positioned as shown for the 4-km interferometer.

Figure 4: Position of PSL/IOO Tables on LVEA in Hanford, WA

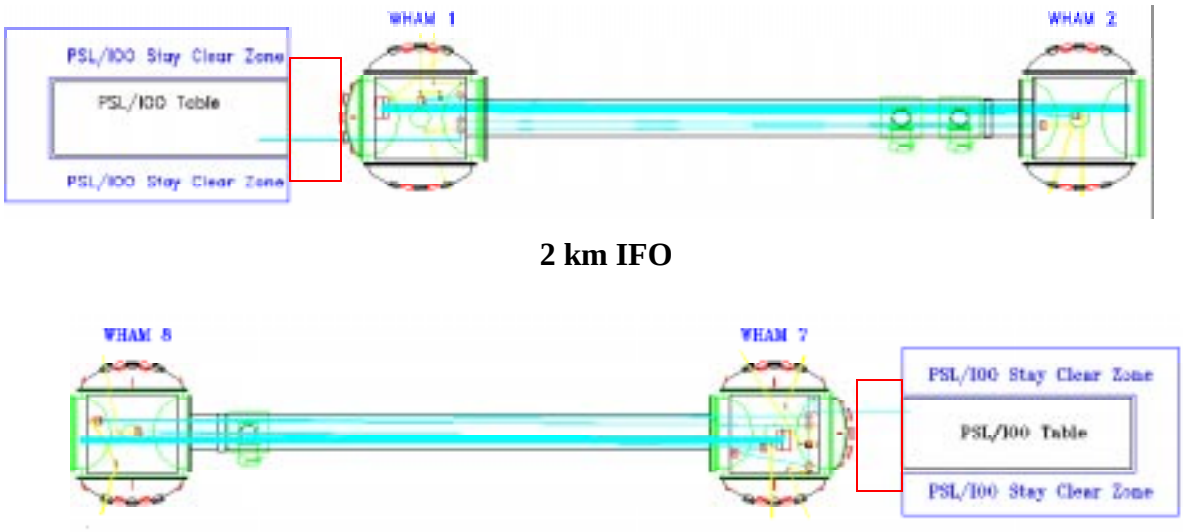

4.2.2. Optical Layout on PSL/IOO Table

All in-air components are located on the PSL/IOO table, including the RF modulation components, the mode cleaner mode matching telescope optics, the periscope raising the beam from the PSL/IOO table to the HAM beam height, and IOO diagnostics. Figure 5 displays the overall layout of the IOO components on the PSL/IOO table.

Figure 5: Detailed Optical Layout of IOO components

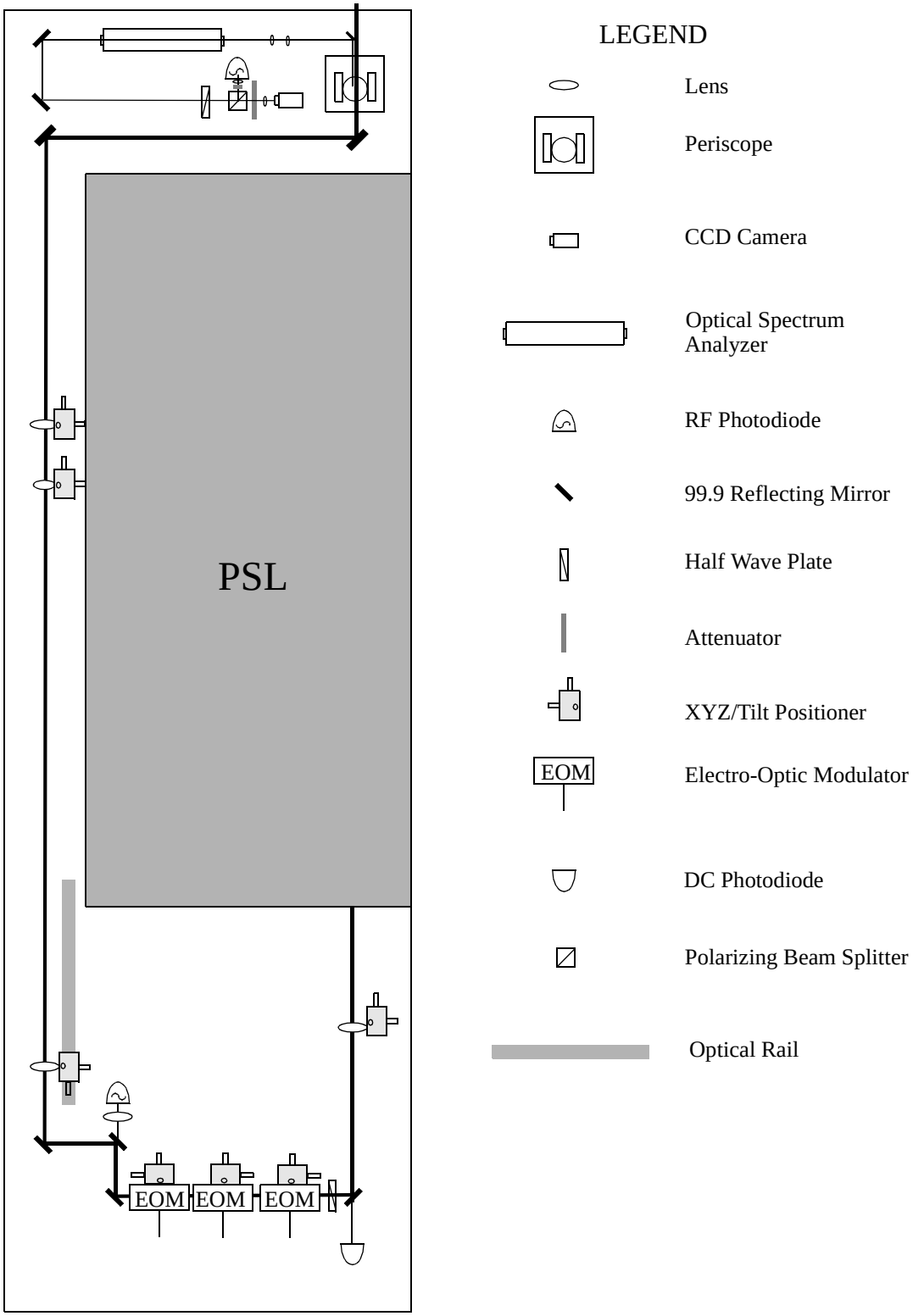

4.2.3. IOO/HAM Interface-Periscope

Since the relative laser beam heights at the IOO/PSL table and at the input port of HAM1 has a 35” rise, a periscope is designed to raise the beam without change of the polarization of the light. The structure of the periscope has to maintain the stability of the supporting table and the lowest resonances have to be high enough to avoid amplification of ground noise. A simple structure comprising two tapered aluminum beams is designed to provide necessary stiffness. Figure 6 shows the dimensions of the basic structure. Mike Fine calculated the lowest 6 resonance frequencies using finite element analysis, which are shown in Table 2. The transfer function of the periscope structure has not been calculated; however since the lowest frequency is above 200 Hz, the transfer function below 100 Hz can be safely assumed to be unity.

Figure 6: Basic structure of the periscope. Material: aluminum

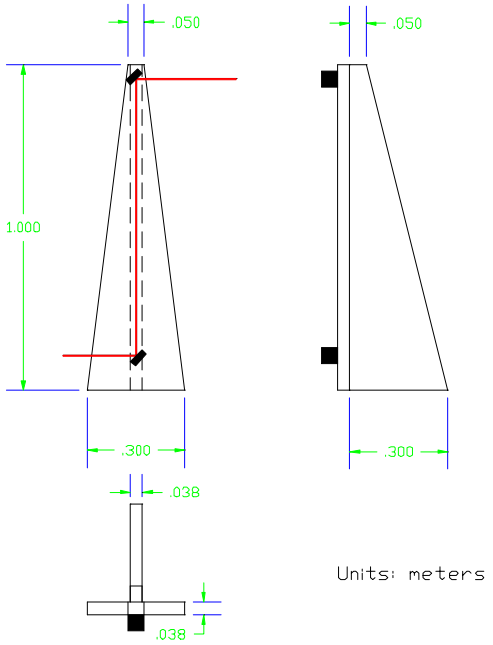

The top of the optical table (RS 4000 Table from Newport is assumed) has a typical maximum relative motion value of $< 1.3 \times 10^{-10}$ m (see Newport catalog). Assuming the top mirror on the periscope has a maximum motion relative to the bottom mirror of 1×10^{-9} m, the output beam direction disturbance caused by this motion is about 2×10^{-9} rad which is negligibly small compared to the laser beam pointing angle fluctuations (in the order of μrad).

The periscope fits under the planned table cover. A hole is required in the cover for the exit beam, with either a nozzle (3-4 inch diameter TBD/PSL) or holes for a flange attachment. A tube will protect the beam between the cover and the HAM viewport.

.

Table 2: Calculated resonance frequencies of the periscope basic structure.

Mode No.	Resonance Frequencies (Hz)
1	203
2	301
3	317
4	659
5	748
6	820

4.2.4. IOO/PSL Vibration Isolation

The PSL/IOO table will be floor mounted using table legs similar to the Newport Research Corporation Model I2000 isolation system. The legs have the capability of floating the table, but seismic noise on the LVEA floor does not compromise the isolation of an unfloated table.

4.3. In-Vacuum Components

The in-vacuum components of the IOO are shown in Figure 7 and Figure 8. The in-vacuum layout of the IOO components was driven by several considerations:

- Mode cleaner length - the requirements on mode cleaner length[1] determine the positions of the SOS in the HAMS
- Scattered light - SYS requires that scattered light loss be limited to 1 ppm intensity clipping in the COC. For all components except for the Faraday Isolator we are able to meet the 1 ppm criterion. The 8 mm diameter of the FI crystal clips at the 20 ppm level.
- Positioning of the MMT mirrors - To be able to achieve the maximum independent adjustibility of the mode parameters into the COC, we require that the mirror MMT 1 be able to move over the length of HAM 1.[2] MMT2 is required to move over a distance proportional to the motion of MMT1 to maintain independent control of mode parameters.
- Minimization of coupling of stray magnetic field (*B*) to the SOS mirror actuators - a minimum separation distance of 20 cm between the FI and the SOS is required to reduce the displacement noise induced on the suspended mirror by *B*-field fluctuations to a level below the ambient displacement noise induced by seismic fluctuations.[3]

The scale layouts for the individual HAMs are shown in the Figures below. Lines representing beams are drawn at the 1 ppm intensity contour. The drawing has been somewhat distorted from the AutoCad layout to fit on the page; the closest this contour comes to the walls is ~ 1 cm where the beam from MMT1 leaves WHAM 1.

1. D. Coyne, *LIGO-T970068-00-D; D. Tanner LIGO-T-970xxx-03-D.*
2. T. Delker, R. Adhikari, S. Yoshida, and D. Reitze, *LIGO-T970143-00-D*
3. S. Yoshida, R. Adhikari, and D. Reitze *LIGO-T970149-00-D.* Analysis of B-field coupling to the SOS magnets assuming that the FI is bolted to the seismic isolation stack.

4.3.1. 4 km IFO

4.3.1.1 WHAM 1

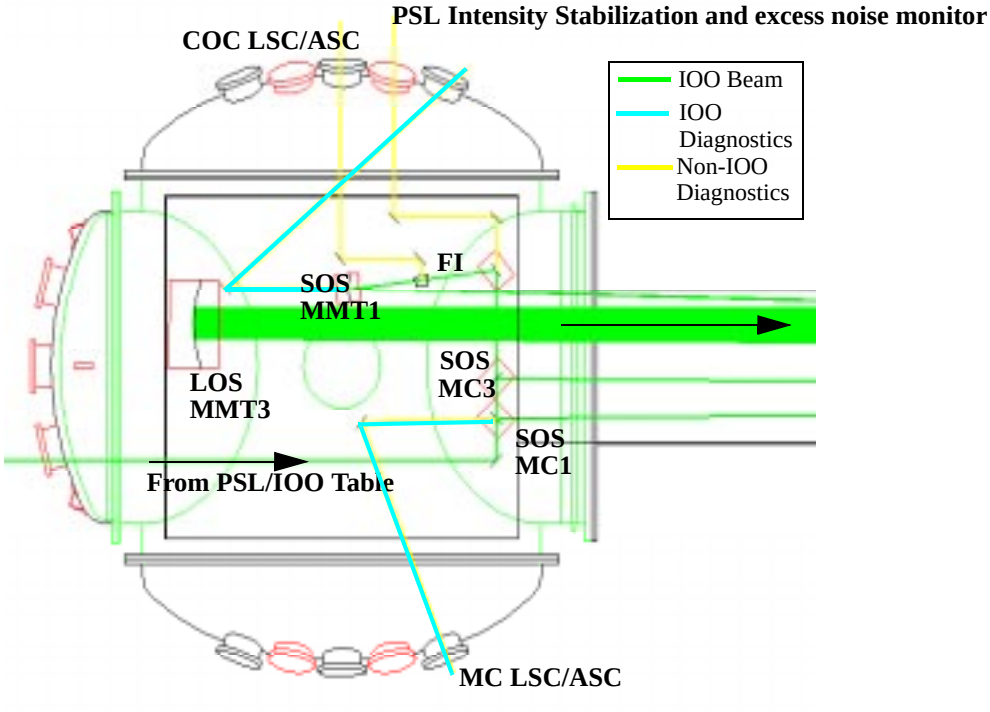

4.3.1.2 WHAM 2

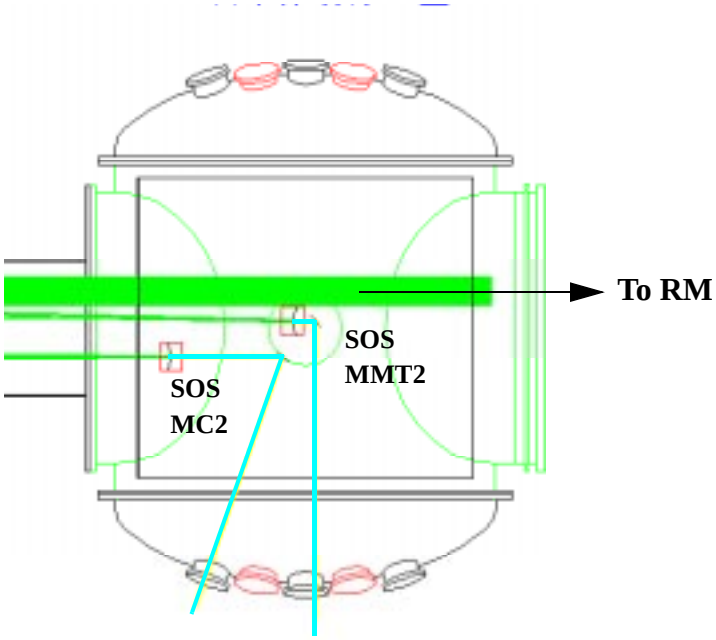

Figure 7: Layout of the 4-km IFO

4.3.2. 2 km IFO

4.3.2.1 WHAM 7

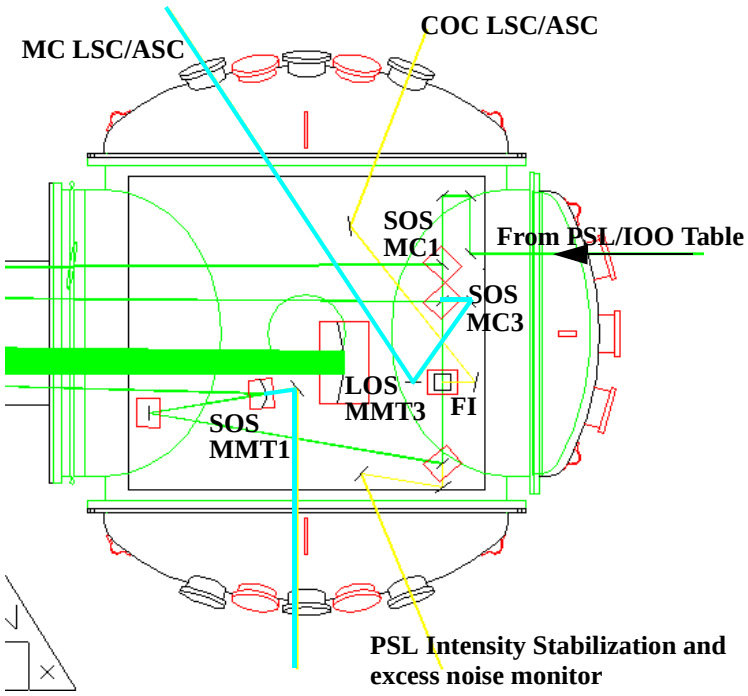

4.3.2.2 WHAM 8

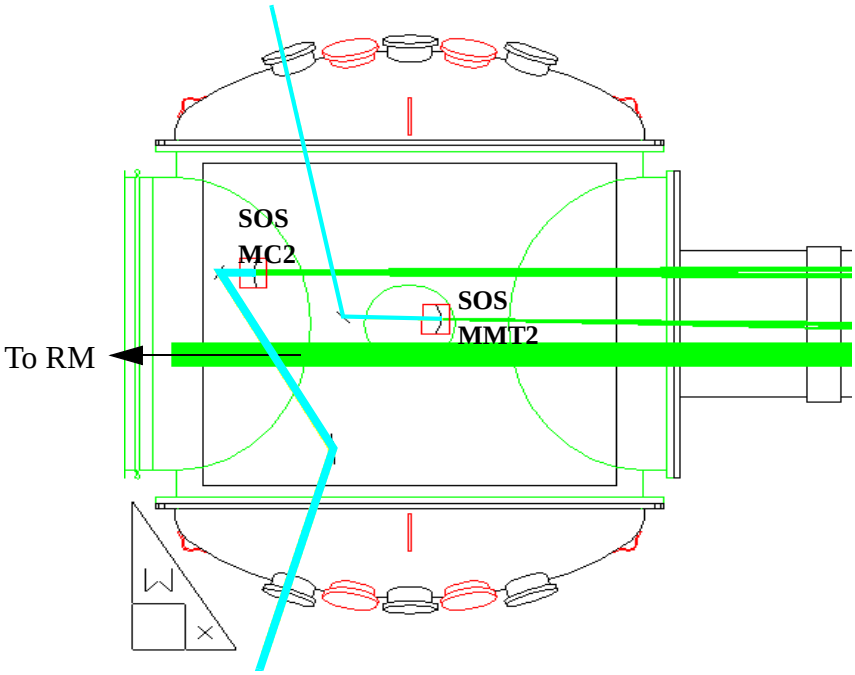

Figure 8: Layout of the 2-km IFO

4.3.3. The In-Vacuum Faraday Isolator

A Faraday isolator positioned between the mode cleaner and the mode-matching telescope serves to divert the back-reflected interferometer light out to ISC photodiodes for IFO diagnostics. The presence of the FI in the vacuum impacts IOO design considerations from a number of stand-points:

- Vacuum Contamination
- Stray B-field coupling to SOS magnets
- Thermal lensing in the FR

The IOO will use an FR with the following characteristics:

- Magneto-Optic Material: Terbium-Gallium-Garnet (TGG)
- Clear Aperture 8 mm (20 ppm intensity aperture)
- FR Transmission: >98% (TBD IOO)
- Optical Isolation: >30 dB
- Isolation Uniformity: TBD IOO
- CW Damage Threshold: > 1 KW/cm^2
- Internal Magnetic Field: 0.7 T

TGG was chosen over terbium-doped glass because it is less absorptive and has higher thermal conductivity. The aperture size was chosen as a compromise between reduced isolation (for larger apertures) and beam clipping (smaller apertures). As part of the FR certification, we will measure the spatial dependence of the isolation with the possibility of going to a larger aperture.

A pair of Brewster thin film polarizers will be used as the polarizing elements in conjunction with the FR:

- Material: BK7
- Clear Aperture: 2.5 cm
- Incident Angle: 57.1 deg.
- Extinction Ratio: 100:1 (Intensity)
- CW Damage Threshold: > 1 KW/cm^2
- FR/Polarizer Transmission: > 92% (Vendor spec; TBD IOO)

Brewster thin film polarizers have greater loss than other types, but can handle the power better.

4.3.3.1 Vacuum Compatibility of the Faraday Isolator

4.3.3.1.1 Vendor Survey

Commercially available FRs use epoxy as part of the manufacturing process. A trade survey of FRs manufacturers gives the following materials:

Manufacturer: Electro-optic Technologies

- Magneto-Optic Material: TGG
- Magnet: Nd:Fe:B (not bakeable, T_{Curie} = 337 C)
- Epoxy: 3M DP460 Epoxy (bakeable)*

- O-rings: Viton VT47 (bakeable)*
- Rod Holder: Brass
- Housing: Aluminum
- Fasteners: Stainless Steel
- Special Features: The FR can be delivered as components (to enable a bake of the epoxied parts) and then assembled

*Can be replaced with user-specified epoxy, O-ring

Manufacturer: Optics for Research (OFR)

- Magneto-Optic Material: TGG
- Magnet: Nd:Fe:B (not bakeable)
- Magnet Cement: TBD
- Epoxy: TBD
- Rod Holder: Brass
- Housing: Aluminum
- Fasteners: Stainless Steel
- Special Features: OFR has manufactured space-certified FIs

4.3.3.1.2 FR Vacuum Certification

The IOO plans to vacuum certify the FR using the standard bake-out protocol and RGA analysis. If it is determined that all hydrocarbon outgassing materials must be eliminated from the FR, both of the companies above have agreed to LIGO-specific redesign of the FR without the use of vacuum contaminants.

4.3.3.2 Stray Magnetic-fields

The Faraday isolator (FI) placed after the mode cleaner has a magnet that generates an intense B (magnetic) field. Part of this B-field leaks out of the FI into surrounding areas. Because of the dynamic displacement of FI due to seismic noise, this stray B-field fluctuates with a frequency and amplitude determined by the combination of the seismic noise and the transfer function of the optical table on which FI is placed. This B-field fluctuation can affect the operation of the magnetic actuators used for nearby mirrors by coupling to the magnets and inducing torques and forces on the suspended optic.

The strength of the B-field around the FI will be measured (**TBD/IOO**) We have computed the effects of a stray B-fields for SOS mirrors[1] assuming:

- FI's seismic vibration represents FI's relative motion to the actuator magnets.
- FI is placed on a vibration isolation stack with viton springs having the horizontal transfer function used by G. Gonzalez[2] and the stack experiences ground noise measured at Livingston, LA.
- The mirror has rotational freedom about its three principal axes as an cylinder.
- B(0) = 0.7 T

---

1. S. Yoshida, *LIGO-T970149-00-D*
2. *Environmental Input to Alignment noise, LIGO-T960103-00-D*

The force F and torque τ that a magnet having a dipole moment μ feels can be written as

$$F = grad(\mu \cdot B) = grad(\mu \cdot B_0) + grad(\mu \cdot B_1)\exp(i\omega t) \equiv F_0 + F_1 \exp(i\omega t) \quad (1)$$

and $$\tau = \mu \times B = \mu \times (B_0 + B_1 \exp(i\omega t)) \equiv \tau_0 + \tau_1 \exp(i\omega t) \quad ,$$

respectively, where $B_0(x, y, z)$ and $B_1(x, y, z)$ are the static and dynamic stray B-field that the magnetic dipole feels:

$$B = B_0 + \left\{ \frac{\partial}{\partial x} B_0 \cdot \Delta x + \frac{\partial}{\partial y} B_0 \cdot \Delta y + \frac{\partial}{\partial z} B_0 \cdot \Delta z \right\} \exp(i\omega t) \equiv B_0 + B_1 \exp(i\omega t)$$

and Δx, Δy, Δz are the amplitude spectral density displacements of the FI on the stack. The Faraday B-fields can be modeled as a solenoid.[1] The on-axis field is shown in Figure 9; however, one must compute the off-axis fields to model accurately the field gradients.

The resulting displacement noise induced on the SOS mirror is shown in Figure 10, which compares the stray B-field induced motion against the open-loop motion of the suspended mirror for a separation distance of 17 cm between the FI and the SOS. In our computation, we have neglected low frequency (< 1 Hz) displacement motion arising from the microseismic peak, since the length scales involved are less than 1 m. At all frequencies, the FI induced displacement noise is comparable to or less than seismic displacement noise. Note the dipole magnetic fields fall off as z^{-3}; thus, placement of the FI at separation distances of 20 cm from the SOS should have negligible impact on the performance of the SOS actuators.

Figure 9: On-axis B-field used in this estimation

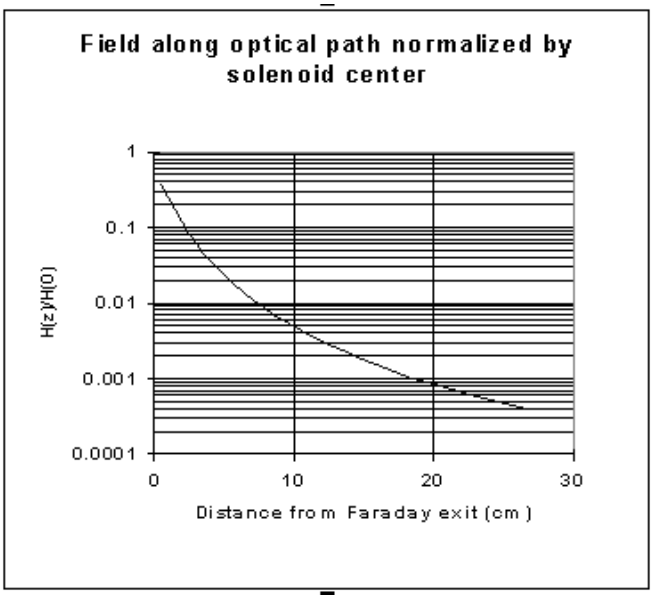

Figure 10: Comparison of B-field-induced and seismic open loop SOS mirror motion

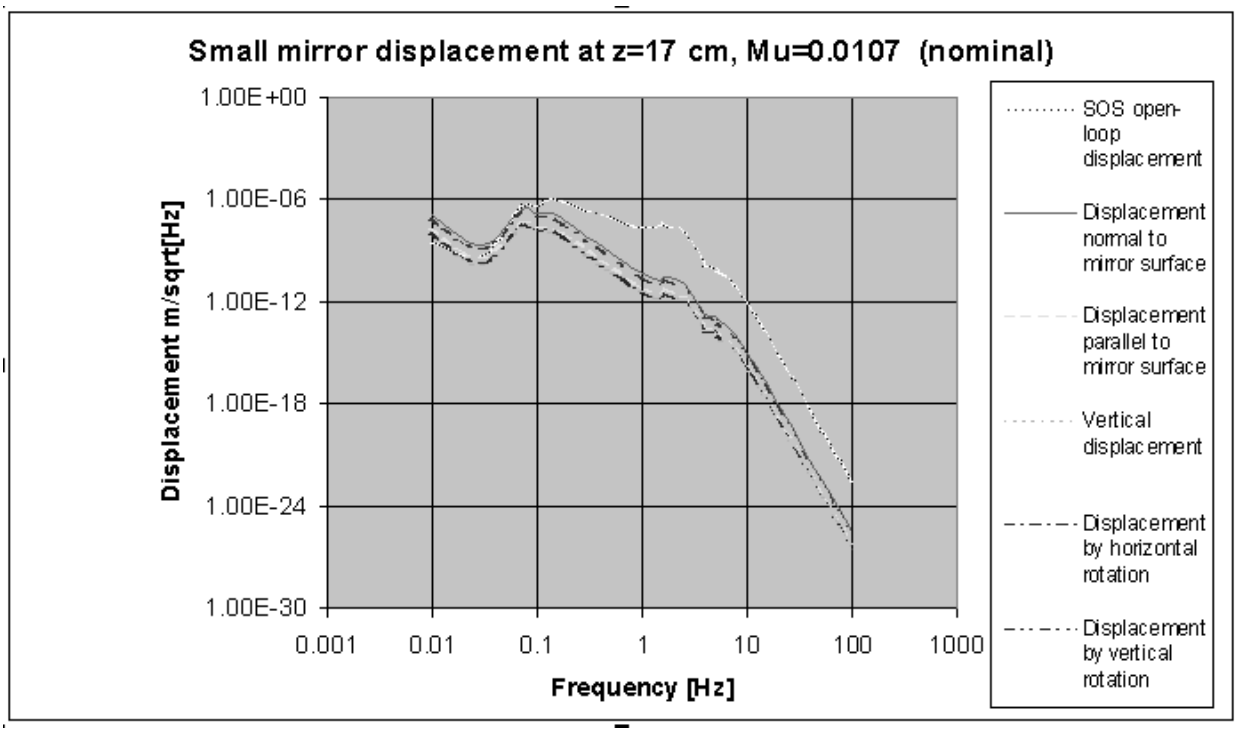

4.3.3.3 Absorption-Induced Thermal Lensing

Thermal lensing is also expected from the Faraday isolator.[1] Since the FI is located after the mode cleaner, any thermal lensing and aberrations introduced by the FI affect the coupling of the beam into the IFO. Since this affects the design of the mode-matching telescope, we defer a discussion of thermal lensing to Section 7.

1. T. Delker, R. Adhikari, S. Yoshida, and D. Reitze, *LIGO-T970143-00-D*

5 RF MODULATION

5.1. Baseline Design

The IOO RF modulation system must provide both the resonant and nonresonant sidebands required by the LSC and ASC subsystems. Two Pockels cells provide phase modulation of the carrier from the PSL. In a change from the IOO Conceptual Design, a simple series arrangement of these cells is used, rather than the Mach-Zender system described in the IOO/CD.

The LIGO ISC employ two modulation frequencies:

1. The first modulation frequency gives upper and lower sidebands that are resonant in the recycling cavity but not resonant in the interferometer arm cavities. These are used for controlling the lengths of the interferometer and for aligning the arm cavities and the beam splitter.

2. The second modulation frequency gives upper and lower sidebands that are not resonant in the recycling cavity. These are used for alignment of the recycling mirror.

The values of these frequencies are set by the lengths of the respective cavities. The resonant sideband frequency must satisfy

$$f_{res} = \left(k + \frac{1}{2}\right)\frac{c}{2L_{rc}}$$

where k = 0,1,2... and L_{rc} is the recycling cavity length. The extra factor of 1/2 occurs because the carrier is resonant in the arm cavities whereas the sidebands are not resonant in the arms, giving a extra 180^{o} phase shift in the reflexivity of the arms.

The nonresonant sideband frequency is chosen to be far from the recycling cavity resonances. Both the resonant and nonresonant sidebands must be equal to one of the mode cleaner resonances, because the RF modulation is imposed before the mode cleaner. The resonant frequencies of the mode cleaner are:

$$f_{mc} = n\frac{c}{2L_{mc}}$$

where n is an integer (1,2,3...) and L_{mc} the mode cleaner length.

The remaining consideration in choice of the modulation frequencies is that they must miss all the harmonics of the arm free spectral range: 37.5 kHz in the 4-km interferometer; 75 kHz in the 2-km interferometer.

5.2. Constraints

The mode cleaner and recycling cavities span vacuum chambers whose separations determine the cavity lengths. There is some flexibility on account of the size of the optical tables in these chambers. The mode cleaner for the 4-km interferometer occupies HAM-1 and HAM-2; the recycling mirror is in HAM-3; the input test masses are in BSC-1 and BSC-3. The mode cleaner for the 2-

km interferometer occupies HAM-7 and HAM-8; the recycling mirror is in HAM-9; the input test masses are in BSC-7 and BSC-8.

In addition to the separations of the vacuum chambers, a number of factors affect the optical lengths of the mode cleaner and recycling cavities. These include the footprints of the suspensions, mirror thicknesses, the triangular path of the mode cleaner, substrate refractive index, the space required for other optical components, the offset of the optical centerline from the centerlines of the beam tubes, and the Schnupp asymmetry of the core optics. These factors have been considered by several workers recently, with similar conclusions.[1]

5.3. Resonant sidebands.

5.3.1. Resonant sideband frequency.

The RF frequencies for the resonant sidebands have been chosen according to the following criteria:

- The frequency must be consistent with the resonant cavity lengths described previously..
- The lengths of the two cavities shall not be an integer multiple of each other.
- The frequency shall be as low as possible.

The design frequencies and lengths (**TBD/SYS**) for the two interferometers are in Table 3:

Table 3: Modulation frequencies for resonant sidebands and corresponding optical lengths (mm).

IFO	*n,k*	f_{res}	L_{mc}	L_{rc}
4-km	2,1	24.493	12240	9188
2-km	3,2	29.486	15251	12715

These frequencies and lengths differ from those given in the IOO/CD. See the documents in footnote 1 for calculations justifying them.

5.3.2. Resonant sideband modulation index.

The modulation index for the resonant sidebands is specified in the SYS document as $\Gamma = 0.47$. The modulation index is to be adjustable over a range of $0< \Gamma<1$ (**TBD/ISC**).

With a nominal 6~W delivered to the core optics, a modulation index of $\Gamma= 0.47$ will provide 5.36 W in the carrier and 310 mW in each first-order sideband. A modulation index of $\Gamma = 1$ will provide 3.51 W in the carrier and 1.16 W in each first-order sideband.

5.3.3. Pockels cell

Phase modulation in a Pockels cell is achieved by electrically varying the optical path length of the light through an electro-optic crystal. The crystal must be aligned with the light polarization in

1. For details see M. Zucker and P. Fritschel, LIGO-T960122-00-I, D. Coyne, LIGO-T970068-00-D, D.B. Tanner, LIGO-T-970xxx-03-D.

order to avoid residual amplitude modulation to within (**TBD/IOO**). By using a resonant device, the RF drive voltages can be kept low. In this configuration, the 50Ω output of the RF amplifier is matched to the capacitive load of the crystal by a resonant circuit. Typical RF bandwidth is 1%, which is larger than the tuning range of the RF generators.

A suitable modulator is MgO:LiNbO3 (New Focus 4003) which has a phase shift of 0.2 rad/Volt. Thus, 4.7 V peak-to-peak is necessary for $\Gamma = 0.47$ and 10 V peak-to-peak for $\Gamma = 1$. The latter voltage implies a power load of 1/4 W RMS from the RF system.

5.4. Nonresonant sidebands.

5.4.1. Nonresonant sideband frequency.

The RF frequencies for the nonresonant sidebands have been chosen according to the following criteria:

- The frequency must be consistent with the mode cleaner cavity lengths described above.
- The frequency shall be sufficiently high that the effect of first-order mixing of the resonant and non resonant sidebands is reduced.
- The frequency shall not be an integer multiple of the resonant sideband frequency.
- The frequency shall be within the demonstrated range of the RF photodiodes (70 MHz TBD-ASC).

The frequencies for the two interferometers are in Table 4.

Table 4: Modulation frequencies for nonresonant sidebands.

IFO	n	f_{nr} (MHz)
4-km	5	61.232
2-km	7	68.800

(Note that these frequencies are not those given in the IOO Conceptual Design and in the SYS document. The SYS document gives the frequencies as TBD; the IOO/CD gave them as 35.86 and 20.34 MHz for the 4-km and 2-km interferometers respectively. Based on the MIT meeting in July ‘97, we are assuming that the nonresonant sidebands can be shifted to these values.)

5.4.2. Nonresonant sideband modulation index.

The modulation index for the nonresonant sidebands is **TBD/SYS**. The IOO/CD used a Mach-Zender interferometer to eliminate the effect of “sidebands on sidebands.” The output amplitude corresponds to a modulation index of $\Gamma = 0.055$ in the present series modulation. With a nominal 6~W delivered to the core optics, a modulation index of $\Gamma = 0.055$ will provide 2.7~mW in each first-order sideband.

5.4.3. Pockels cell performance

The Pockels cell for the non resonant sideband will be identical to the one used for the resonant sideband. The voltage for Γ = 0.055 is below 0.6 V peak-to-peak, making the RF power required 0.9 mW.

5.5. Modulation cross products.

The output of the RF modulation section will be phase-modulated light, of the form

$$E = e^{-i\omega t + i\Gamma_1 \cos(\Omega_1 t) + i\Gamma_2 \cos(\Omega_2 t)}$$

where ω is the infrared frequency of the carrier, Γ is the modulation index and Ω_i is the frequency of the i^{th} sideband. This formula can be expanded using

$$e^{i\Gamma\cos(\Omega t)} = J_0(\Gamma) + 2i\sum_{k=1}^{\infty}(-1)^{k-1}J_{2k-1}(\Gamma)\cos[(2k-1)\Omega t] - 2\sum_{k=1}^{\infty}(-1)^{k-1}J_{2k}(\Gamma)\cos[2k\Omega t]$$

When this is written out, one sees that with two modulation frequencies, there will be output at sums and differences of Ω_1 and Ω_2. The frequencies and amplitudes of these "sidebands on sidebands" are given in Table 5.[1] We have listed all intermodulation products above 10^{-9} in amplitude for frequencies up to the non-resonant sideband Ω_2, and all products above 10^{-7} up to2.5 times this frequency. (For simplicity we take 25 and 62.5 MHz as the 4-km interferometer modulation frequencies; 30 and 80 MHz as the 2-km frequencies. The input light has unit amplitude.) We have also listed whether the products are in phase or in quadrature with the carrier and whether the new frequency will be admitted by the recycling cavity or not.

Table 5: RF sideband frequencies.

Product	*Phase*	*4-km*		*2-km*		*Amplitude*
		MHz	RC admit Admit	MHz	RC admit	
Carrier	Re	0	Y	0	Y	0.945
$5\Omega_1 - 2\Omega_2$	Im	0	Y	10	N	2.24×10^{-9}
$\Omega_2 - 2\Omega_1$	Im	12.5	N	20	N	7.45×10^{-4}
$3\Omega_1 - \Omega_2$	Re	12.5	N	10	N	5.86×10^{-5}
Ω_1	Im	25	Y	30	Y	0.228

1. *Impact of Non-resonant Sidebands on Length Sensing Signals*, J. Camp, LIGO-T970097-00-D

Table 5: RF sideband frequencies.

Product	*Phase*	*4-km*		*2-km*		*Amplitude*
		MHz	RC admit Admit	MHz	RC admit	
$2\Omega_2 - 4\Omega_1$	Re	25	Y	40	N	4.75×10^{-8}
$\Omega_2 - \Omega_1$	Re	37.5	N	50	N	0.00628
$4\Omega_1 - \Omega_2$	Im	37.5	N	40	N	3.45×10^{-6}
$2\Omega_1$	Re	50	N	60	N	0.0271
$2\Omega_2 - 3\Omega_1$	Im	50	N	70	N	8.06×10^{-7}
Ω_2	Im	62.5	N	80	N	0.0256
$5\Omega_1 - \Omega_2$	Re	62.6	N	70	N	1.62×10^{-7}
$3\Omega_1$	Im	75	Y	90	Y	0.00213
$2\Omega_2 - 2\Omega_1$	Re	75	Y	100	N	1.02×10^{-5}
$\Omega_1 + \Omega_2$	Re	87.5	N	110	N	0.00628
$4\Omega_1$	Re	100	N	120	N	1.25×10^{-4}
$2\Omega_2 - \Omega_1$	Im	100	N	130	N	8.64×10^{-5}
$2\Omega_1 + \Omega_2$	Im	112.5	N	140	N	7.45×10^{-4}
$2\Omega_2$	Re	125	N	160	N	3.57×10^{-4}
$5\Omega_1$	Im	125	N	150	Y	5.91×10^{-6}
$3\Omega_1 + \Omega_2$	Re	137.5	N	170	N	5.86×10^{-5}
$\Omega_1 + 2\Omega_2$	Im	150	N	190	N	8.64×10^{-5}

RF photodiodes produce signals proportional to the light intensity or field squared. (The intensity, in turn, depends on the highly dispersive behavior of the interferometer.) The key frequency is Ω_1, 25 MHz in the case of the 4-km interferometer. The other key factor is whether the *E*-field is admitted by the recycling cavity. Most of the intemodulation products are not admitted into the recycling cavity, so their amplitude at the dark port is reduced by the transmission of the recycling mirror The contributions to the RF power at 25 MHz (which is incindent towards the beam splitter, assuming 6 W in the carrier) are given in Table 6

Table 6: Power at 25 MHz in 4-km instrument.

Mixing of	*Admitted to RC*	*Power (W)*
$(2\Omega_2 - \Omega_1) - 3\Omega_1$	$3\Omega_1$	9.25×10^{-8}
$(2\Omega_2 - 3\Omega_1) - \Omega_1$	Ω_1	9.25×10^{-8}

Table 6: Power at 25 MHz in 4-km instrument.

Mixing of	*Admitted to RC*	*Power (W)*
$(\Omega_2 - 2\Omega_1)^2$	No	4.68×10^{-8}
$(\Omega_2 - \Omega_1) - (3\Omega_1 - \Omega_2)$	Neither	3.11×10^{-8}
$2\Omega_2 - 4\Omega_1$	Neither	1.13×10^{-8}
$\Omega_2 - (4\Omega_1 - \Omega_2)$	Neither	7.53×10^{-9}
$(3\Omega_1 - \Omega_2) + (\Omega_2 - 2\Omega_1)$	Neither	3.67×10^{-9}

By comparison, shot noise on 6 W is 1.06×10^{-9} W/rHz. The worst cases are $(2\Omega_2 - \Omega_1) - 3\Omega_1$ and $(2\Omega_2 - 3\Omega_1) - 1\Omega_1$. These essentially are the same product, and are about 10x shot noise at 100 Hz.The square of the relatively strong sideband at 12.5 MHz also is significant.

All would be reduced below shot noise if the nonresonant sideband were raised to approx. 87 MHz.

6 THE MODE CLEANER

The mode cleaner has several purposes in LIGO. It filters the non TEM_{00} components of the PSL output light, reduces amplitude and frequency noise of the light, contributes to frequency stability of the laser, decreases beam wiggle, and filters any s-polarized component introduced by the optics in front of it.

6.1. Mode cleaner characteristics.

The mode cleaner is essentially a Fabry-Perot cavity with a high (several thousand) finesse. A simple Fabry-Perot cavity has transmission

$$t = \frac{t_1 t_2 e^{i\delta}}{1 - r_1 r_2 e^{2i\delta}}$$

where t_1 is the amplitude transmission and r_1 the amplitude reflectivity of the input mirror; t_2 is the amplitude transmission and r_2 the amplitude reflectivity of the output mirror; δ is the optical phase associated with the cavity half-length L; for plane waves and plane-parallel mirrors, $\delta = 2\pi\nu L/c$ where ν is the frequency of the light. The resonator has transmission maxima whenever $\delta = n\pi$, with n an integer.

The mode cleaner in LIGO is a ring Fabry-Perot resonator in the shape of a narrow isosceles triangle. Two plane mirrors define the base and a curved mirror is located at the apex of the triangle. The triangle configuration is preferred for several reasons, notably the much improved optical isolation it provides[1] .

The mode cleaner is located in vacuum, with the plane mirrors in HAM1 (4 km) and HAM7 (2 km) and the curved mirror in HAM2 (HAM8). The separation between these chambers determines the free spectral range of the mode cleaner, as discussed in section 5 and elsewhere. The mode cleaner mirrors are suspended by a single loop of wire using a Small Optics Suspension (SOS).

The specific features of the mode cleaner are discussed in the following paragraphs.

6.1.1. Polarization dependence.

The mode cleaner transmits only one polarization of the light.[1] Because the mode cleaner has an odd number of reflections during one round-trip circuit, the overall phase of s-polarized light (E normal to plane of the cavity) is reversed on one circuit. This shifts the resonance condition from the usual $\nu = cn/2L$ to

$$\nu = \frac{c}{2L}\left(n - \frac{1}{2}\right)$$

1. *Estimation of Special Optical Properties of a Triangular Mode Cleaner,* F.J. Raab and S.E. Whitcomb, LIGO Technical Note #108 (1992).

The phase reversal does not happen for p-polarized (*E* in the plane) light. Thus the mode cleaner acts as polarization sensitive filter. As its length is varied, first one and then the other polarization is transmitted. We choose s-polarized light for the mode cleaner.

6.1.2. Rejection of high-order modes.

For TEM_{lm} Gaussian modes, the resonances occur at frequencies

$$\nu_{lm} = \frac{c}{2L}\left[n - \frac{1}{2} + \frac{l+m+1}{\pi}\operatorname{acos}(\sqrt{g})\right]$$

where $g = 1\text{-}L/R$ with R the radius of curvature of the curved mirror. The resonator is adjusted for resonance with the TEM_{00} mode; this sets the value of n (of order 10^7). The radius of curvature (and hence g) is chosen so that the resonance condition is not satisfied for $l \neq 0$ and $m \neq 0$ for any $\{n,l,m\}$. The condition is

$$\frac{l+m}{\pi}\operatorname{acos}\sqrt{g} \neq integer + \varepsilon$$

where ε specifies the amount the higher-order mode avoids being resonant. It has been assumed that the actual frequency from the laser of the fundamental and all higher-order modes is the same.

6.1.3. Beam dewiggling.

Beam wiggle (angular and lateral deviations of the beam) may be viewed as the superposition of higher-order Gaussian modes on the TEM_{00} mode.[1] Because higher-order modes are suppressed by the mode cleaner, beam wiggle is suppressed by the mode cleaner. The amplitude of the beam wiggle is suppressed by

$$S_{lm} = \frac{1}{\left[1 + \left\{\frac{2F}{\pi}\sin[(l+m)\operatorname{acos}(\sqrt{g})]\right\}^2\right]^{\frac{1}{2}}}$$

where F is the finesse of the cavity. Since, as already discussed, the quantity $(l+m)\operatorname{acos}(\sqrt{g})$ is chosen *not* integer times π, the value of the sinusoid is not zero. If we take it to be a typical value, 1 rad, then, since $F \gg 1$,

$$S_{lm} \approx \frac{\pi}{2F\sin(1)}$$

1. *Do wiggle effects depend on mode cleaner length,* A. Abramovici, LIGO Technical Note #20 (1988).; *Optical mode cleaner with suspended mirrors,* A. Araya *et al.*, Appl. Opt. **39**, 1446 (1977).

6.1.4. Laser noise suppression.

The mode cleaner acts as a low-pass filter, with a corner frequency of $2\pi/\tau_s$, where $\tau_s = LF/c$ is the storage time of light in the cavity. Amplitude and frequency noise at frequencies higher than the corner frequency are suppressed at a rate of 20 db/decade.

6.1.5. Laser wavelength stabilization.

The mode cleaner can serve as a length standard for the laser. The arms are better standards, so in normal operation, the mode cleaner length is slaved to the laser, but during lock acquisition, the laser may be slaved to the mode cleaner.

6.1.6. Circulating power.

Being a resonant cavity, the stored power in the mode cleaner is larger than the incident power by $1/T$, with T the (power) transmittance of the input and output couplers.

6.2. Optical parameters of the mode cleaner.

Table 7 lists the optical parameters chosen for the mode cleaners. The length L differs for the 4-km and 2-km interferometers because of the differences in the separation of their HAM chambers. The parameters for the 2-km interferometer are then an appropriately scaled version of those for the 4-km interferometer.

Table 7: Optical parameters for the mode cleaners

		4K IFO	2K IFO
Plane mirror transmittance		0.002	0.002
Plane mirror reflectance		0.998	0.998
Curved mirror transmittance		1E-05	1E-05
Mirror absorbance/scattering	each	0.00010	0.00010
Finesse		1550	1550
Free spectral range	MHz	12.246	9.829
Full width/half max	kHz	7.83	6.26
Full width/half max	nm	0.342	0.427
Cavity optical half-length	mm	12240	15251
Mirror thickness	mm	25	25
Mirror wedge angle	mrad	8.73	8.73
Mirror diameter	mm	75	75
Coating diameter (curved mirror)	mm	25	28
Curved mirror radius of curvature	mm	17250	21500
g = 1 - L/R		0.290	0.291
waist size	mm	1.629	1.818
Raleigh range	m	7.83	9.76
Beam divergence	μrad	208	186
spot at flat mirror	mm	1.629	1.819
spot at curved mirror	mm	3.022	3.373
1 ppm intensity, curved mirror	mm	15.9	17.7
Circulating power	kW	4	4
Intensity at flat mirror	kW/cm^2	48.0	38.5
Intensity at curved mirror	kW/cm^2	13.9	11.2

6.3. Mode cleaner performance.

Figure 11 shows the calculated (intensity) transmittance of the mode cleaner as a function of frequency. The calculation is done for the 4-km interferometer. The RF modulation sidebands will be in the second and fifth transmission maximum.

Figure 11: Transmittance of the mode cleaner for the 4-km interferometer.

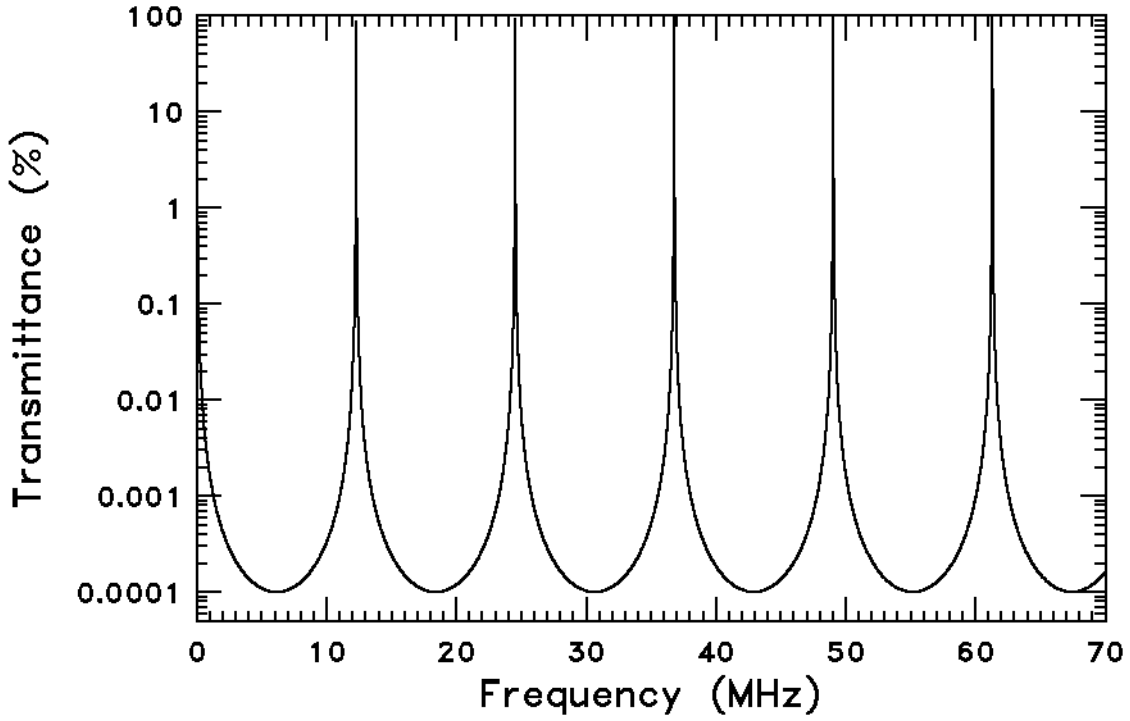

Figure 12 shows the transmission near the peak as a function of frequency (at constant length) and as a function of length (at constant frequency) The full width at half maximum is about 8 kHz and about 0.3 nm. Figure 13 shows the phase change of the transmitted light as a function of frequency and length. The central slope is 0.25 mrad/Hz and 6 mrad/pm.

Figure 12: Transmittance (power) of mode cleaner near the resonance. Left panel shows transmittance as a function of frequency; right as a function of length.

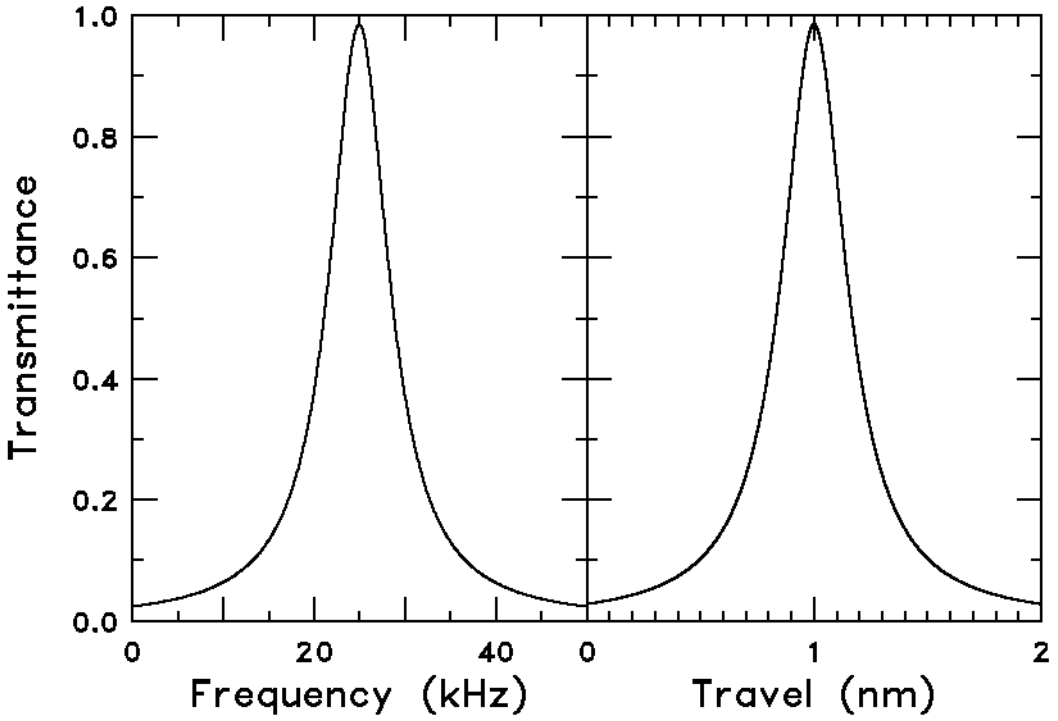

Figure 13: Phase Shift near Resonance of 4 km Mode Cleaner. Left: phase versus frequency; right: phase vs. length.

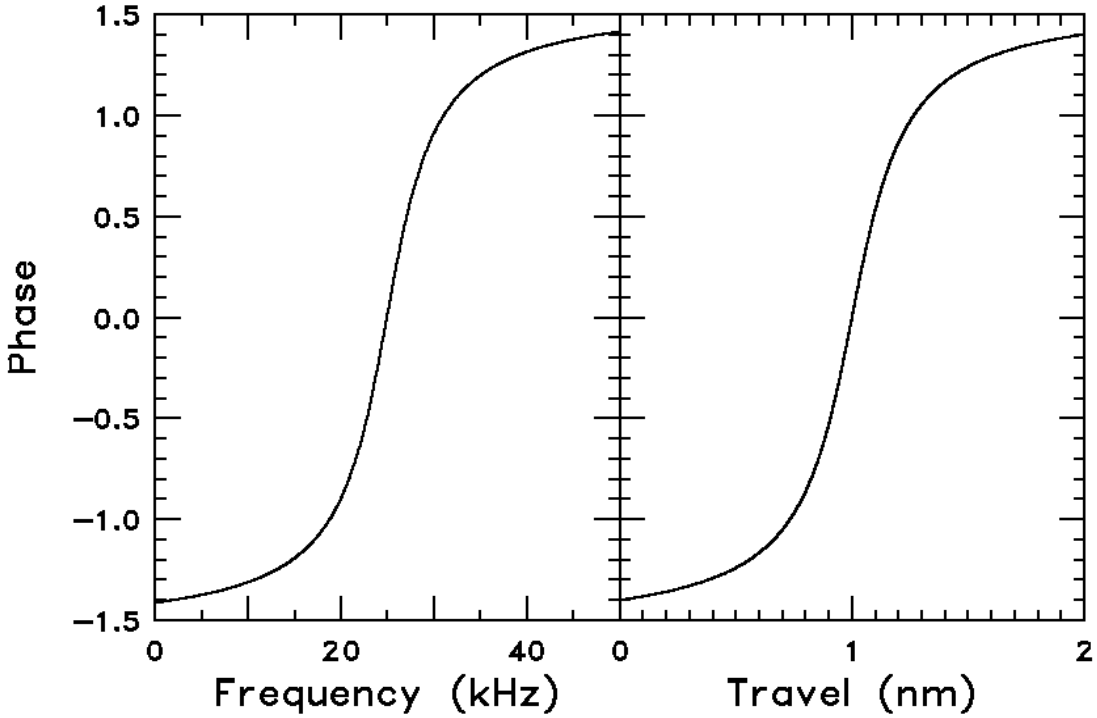

6.3.1. Rejection of the higher order modes.

The value of $g = 0.29$ was chosen by considering the transmission of higher order modes. Figure 14 shows the electric field amplitude transmitted by the mode cleaner under the assumption that it is illuminated with single frequency light with many higher-order modes present in the beam. (In order to avoid having an excessive number of points, the calculation was done for a finesse of $F \approx 100$.) The amplitude of the higher-order modes in the input beam was assumed to fall as $1/\sqrt{l+m}$. In addition, the finite size of the coating on the curved mirror was taken into account in the following way. The linear size of higher-order modes follows $\sqrt{l \times m}$. For the size of the coating on the curved mirror, this means that modes with index bigger than 5 will spill over the high-reflectance area at the 200 ppm level, leading to an effective reduction in the finesse of the cavity. We assumed that modes with ($l+m > 10$) would suffer this loss, initially as

$1/\sqrt[4]{l+m}$ up to $l+m = 15$, as $1/\sqrt{l+m}$ up to $l+m = 20$, and as $1/(l+m)$ thereafer.

The large isolated peak at $g = 0.25$ is from the TEM_{21} and TEM_{30} modes. Other strong peaks include $l+m = 5$ at $g = 0.096$, $l+m = 7$ at $g = 0.38$, and $l+m = 4$ at $g = 0.5$.

The modes are quite crowded for some values of g and rather sparse for others. In particular, there are is a relatively wide gap on either side of the peak at $g = 0.25$. The operating point was chosen in this gap; g was chosen larger than 0.25 so that thermal effects, which will tend to increase the radii of curvature, move the mode cleaner away from the strong maximum at g = 0.25. For circulating power of 4 kW, we estimate that the sagitta of the MC cavity mirrors will change by ~0.1 nm, corresponding to a change of the cavity g-factor from 0.290 (0.291) to 0.291 (0.292) for the 4 km (2 km) MC.

Because the calculation was done for $F = 100$, the transmission at the operating point in Fig. 14 is higher than for the high finesse the mode cleaner will have. The computed transmission for key modes for $F = 1550$ is:

- TEM_{01}, TEM_{10}: 0.0012 in amplitude, 1.4 ppm in intensity.
- TEM_{30}, TEM_{21}: 0.0043 in amplitude; 18 ppm in intensity.

Figure 14: Higher Order Mode Transmission of 4 km IFO

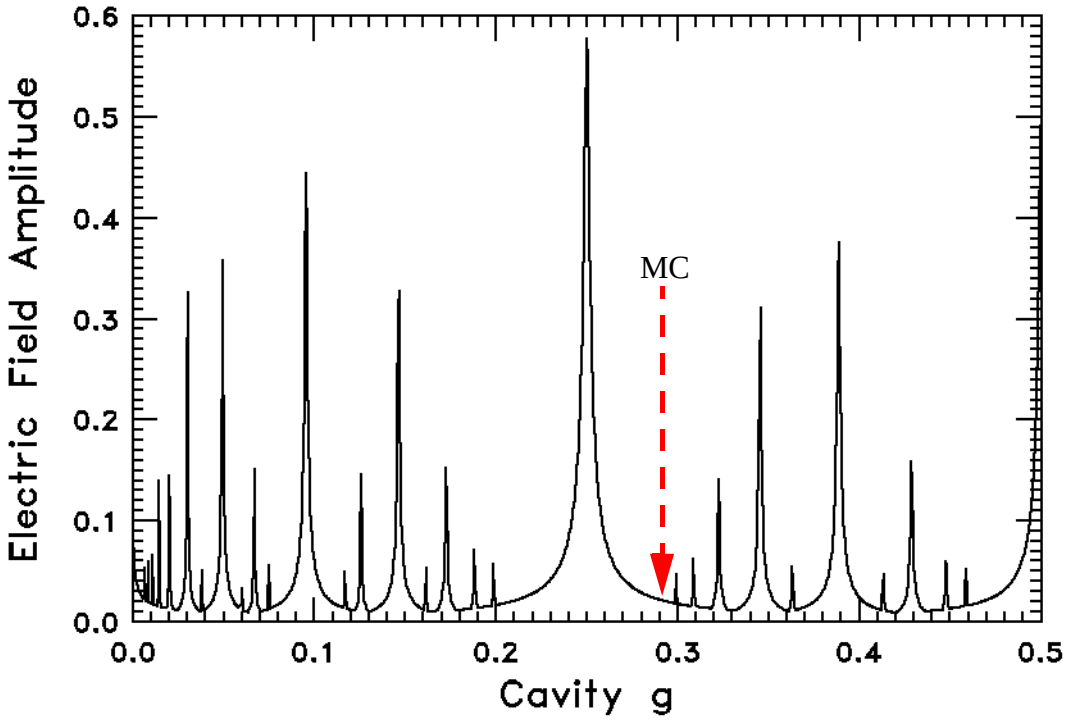

6.3.2. Wiggle and noise suppression.

Beam wiggle will be suppressed by a factor of typically 600 by the mode cleaner. Above the corner frequency of 6 kHz, laser noise is suppressed as 1/*f*.

6.4. Mode cleaner length control

The IOO incorporates the following design choices for the mode cleaner length control, explained below.

- Reflection PDH lock of light to the mode cleaner
  - Sideband modulation index of 0.15
  - Frequencies in Table 7.
  - Modulation cross products down by factor 10^4 compared to resonant sideband
- No active control of sideband tuning to mode cleaner resonance
  - Sideband detune does not couple to GW noise for Q demodulation
  - Stack drift ~ 100 Hz / day after 20 days load
  - Periodic monitor of detune by ~ 10^{-1} Hz dither of laser frequency, looking at induced signal on 50 mW pickoff

These choices are the simplest implementation of the length control consistent with LIGO requirements.

6.4.1. IOO Requirements

6.4.1.1 Frequency stability (limited by MC thermal noise)[1]

3×10^{-5} Hz / rHz 100 Hz

3×10^{-6} Hz / rHz 10 kHz

6.4.1.2 Allowable sideband detune from resonance

100 Hz

This requirement was derived to hold RF oscillator phase noise to amplitude modulation after the mode cleaner at the level of 10^{-8} / rHz[2].

6.4.1.3 Fringe control

10^{-13} m

This requirement was derived to limit excess noise on the light after the mode cleaner to 10% shot noise on 0.5 W light[3].

6.4.2. IOO Performance

6.4.2.1 Loop gains and servo topology

Mode cleaner length control loop gains are TBD. The servo topology will follow that given in the documents *Frequency Stabilization in LIGO,* T960164, and *Frequency Stabilization: Servo Configuration and Subsystem Interface Specification,* T970088

6.4.2.2 Shot noise

With a modulation index of 0.15 (J_1=0.02), and a cavity visibility of 0.99 (100 mW incident on the photodetector), the shot noise limited frequency stability is[4]

3×10^{-6} Hz / rHz 100 - 10 kHz

1. Mode Cleaner Noise Sources, T960165
2. LSC DRD, T960058
3. Secondary Light Noise Sources in LIGO, T970074
4. Mode Cleaner Noise Sources, T960165.

6.4.2.3 Frequencies

We.choose frequencies that are larger than the resonant sidebands, which have all harmonics nonresonant in the mode cleaner, and which have mixing sidebands with both resonant and nonresonant sidebands which are nonresonant in the mode cleaner.

Table 8: Modulation frequencies for mode cleaner locking.

IFO	f_{lock} (MHz)
4-km	33.289
2-km	26.717

6.4.2.4 Modulation cross products from reflection lock sideband

The modulation cross products of the mode cleaner locking sideband will be non-resonant in the mode cleaner and will be attenuated (in power) by a factor of 1000. Thus the amplitude of any cross products will be down by a factor of ~10^4 relative to the GW signal sideband.

6.4.2.5 Sideband detuning from resonance

Sideband detuning from mode cleaner resonance does not couple to noise at the GW port[1]; however it is sensible to maintain the requirement listed above on sideband detuning to limit excess noise on the light, which may cause noise in ways that are unpredicted.

A requirement of a sideband frequency offset from resonance of 100 Hz corresponds to a mode cleaner length stability of ~0.05 mm. After 20 days of load, the stacks will drift at this level over a day span. We propose no active control of the sideband frequency relative to the mode cleaner length; instead an RF photodiode will periodically monitor the amount of excess noise (on 50 mW picked off light) induced by a laser frequency dither coupled to a frequency detune, and frequency and/or length adjustments will be made manually when necessary. With a a 100 Hz detune and a frequency dither of ~0.1 Hz, the excess noise will be ~20 dB above shot noise on 50 mW light.

6.5. Mode Cleaner Alignment

6.5.1. Initial Alignment

The initial alignment will begin with the installation of the in-vacuum chamber components. ASC is to provide position information in the chambers, such that a fiducial point on an optical component can be located within a distance TBD/ASC. For the input optics an accuracy of 1 mm is sufficient, *except for the length of the mode cleaner.* For this, we will need to know the separation of the tables in HAM-1 and HAM-2 to 0.1 mm. (The distance between the inside edges of the tables at two points separated by the diameter of the beam tube connecting them would be the most convenient.)

1. *Secondary Light Noise Sources in LIGO, LIGO-T970074-00-D*

Assuming that the separation is known to the above accuracy, IOO will provide assembly jigs that will allow placement of the optics relative to the edges of the tables to an accuracy of ±0.05 mm and ±0.1 mrad (assuming machine-shop tolerances of 0.002 inch). Accumulated errors in positioning the mode cleaner and telescope optics would then be of order 0.2 mm and 0.04 mrad, corresponding in the former case to an error of 200 Hz in the free spectral range.

The length measurement will be refined by locking the mode cleaner in vacuum and applying a second modulation frequency using one of the IOO Pockels cells. Adjustment of this frequency until the sidebands are transmitted will allow the free spectral range to be measured. The positions will be corrected by adjustments of the assembly jigs.

If the separation is not known to sufficient accuracy, a specific value will be assumed, and the above mentioned free spectral range measurement will provide a correction.

6.5.2. Detection Mode

Alignment requirements on the mode cleaner are set by angular fluctuations of the test masses and of the input beam with respect to the mode cleaner optical axis:

- Centering Tolerance on Mirror:[1] 3 mm
- Input Angle Alignment Tolerance (99% TEM_{00}): 2×10^{-5} rad
- MC Mirror Alignment Tolerance relative to MC optical axis:[2] 3×10^{-7} rad
- Open Loop SOS Displacement Noise: see Fig. 10.

The 3 mm centering tolerance requirements should be satisfied upon initial alignment using visual inspection of the alignment beam as a guide. On-line monitoring of the beam spot on MC mirrors is accomplished by ASC cameras.

Low frequency relative motion between PSL/IOO table and HAM1 and the laser pointing angle fluctuation will cause misalignment of the input beam and the mode cleaner. This misalignment will be detected by the wavefront sensing system and the signal will be used to control the two mirrors on the periscope to maintain optimal coupling to the mode cleaner. To meet the mode cleaner alignment requirement of 2×10^{-5} rad, an open loop gain < 10 at 1 Hz is required for the control loop. PZT stacks will be used as actuators for the control of the mirror pointing.

The MC WFS will be configured as shown below:[3]

1. *Alignment Sensing/Control Design Requirements, LIGO-T952007-03-I*
2. *Input Optics Design Requirements, LIGO-T960xxx-00-D*
3. *Alignment Sensing/Control Preliminary Design, LIGO-T970060-00-D*

Figure 15: WFS Control of MC

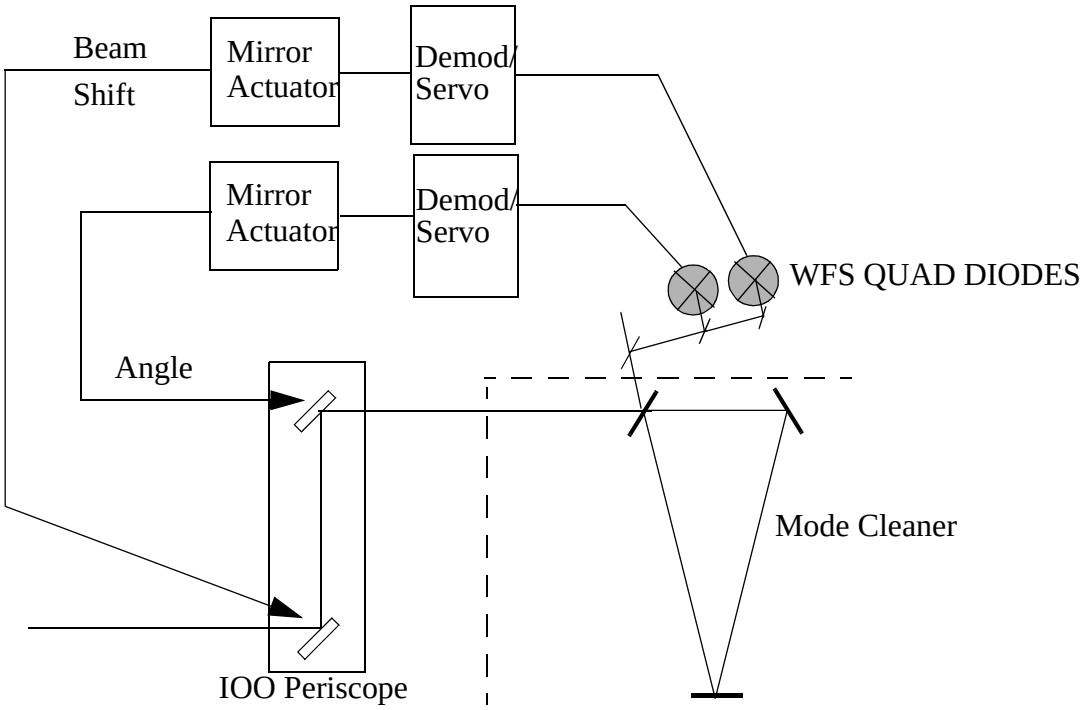

The correction signals from the WFS will be sent to the optics mounted on the IOO periscope. The actuation range is determined by the stack drift relative to PSL/IOO table. For an initial settling drift of 100 μm/day and a logarithmic reduction with time, we assume that 500 μm of beam shift and 5 x 10^{-4} rad of angular shift is adequate to maintain alignment over several lock cycles of the MC without requiring manual re-alignment.

- Angular dynamic range of the periscope: 5 x 10^{-4} rad
- Displacement dynamic range of the periscope: 500 μm
- Actuators: PZT stacks applied to gimbaling of periscope mirrors (*e.g.*, Piezo Systems, Inc.)
  - Response: 0.1 μm/V
  - Required dynamic range: 5 μm (assumes 0.5” actuator displacement from center of optic)
  - Available travel 10 μm.

6.6. Mode Cleaner Mode Matching Telescope

The mode-matching optics indicated in Figure 16 is a three-lens arrangement which allows the waist of the PSL to be matched to the Gaussian parameters of the mode cleaner. Using 3 elements, it is possible to control independently the waist position and the waist size.

Figure 16: Mode Matching Telescope for Mode Cleaner

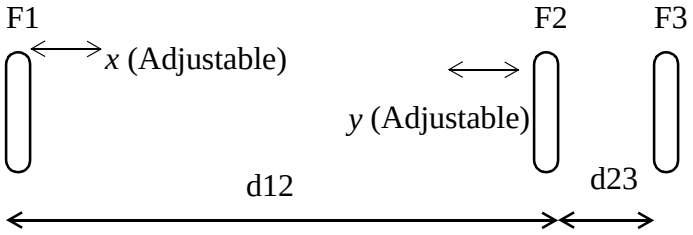

The three-lens design allows for independent adjustment of waist position and waist size. Essentially, x and y are moved in one manner to adjust waist position and in a different manner to adjust waist size. Figures 17 and 18 show these two behaviors. Table 9 gives the parameters of the telescope.

Figure 17: Waist Position Adjustment

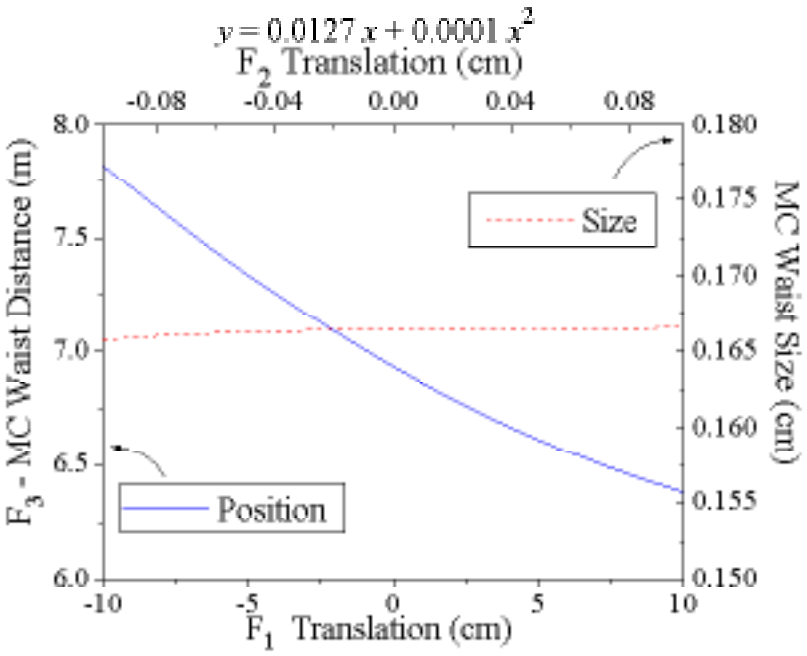

Figure 18: Waist Size Adjustment

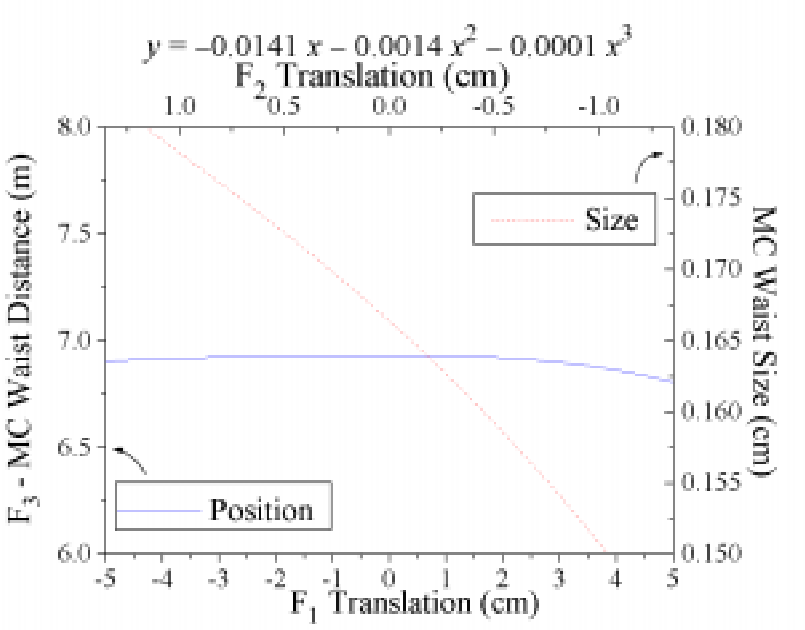

Table 9: Mode matching for the 4-km mode cleaner

Component	
F_1 focal length (cm)	+ 100
F_2 focal length (cm)	- 9.41
F_3 focal length (cm)	+ 28.8
EOM waist size (cm)	0.05
EOM waist - F_1 distance (cm)	93.6
d_{12} (cm)	116.4
d_{23} (cm)	20.1
nominal F_3 - MC waist distance (m)	6.9

7 IFO MODE-MATCHING TELESCOPE

SYS requires that the light from the PSL be coupled into the COC with 95% efficiency (carrier and sideband) (**TBD ASC**). The IOO MMT serves two purposes:

- Maximize the coupled TEM_{00} power (carrier and sideband) in the COC
- Provide steering of the beam from the mode cleaner into the COC

The telescope design must be sufficient to compensate for variations in COC/IOO optics. In addition, the telescope design must provide for diagnostic measurement of the mode-matching.

We have examined the design of the MMT in detail using both analytical methods (ABCD propagation, mode-matching calculations) where possible coupled with optical modeling routines (ASAP, CODE V).[1]

7.1. Expected variations in COC and IOO parameters

Variations from nominal design and operation of the COC and IOO optical components can lead to a reduction in mode-matched power to the COC. Expected deviations which may reduce coupling efficiency include:

- Thermal distortions in COC, mode cleaner, Faraday isolator
- Surface figure errors in polishing of IOO and COC mirrors
- Long term stack drift
- Pump down shifts in the stack positions

7.1.1. Thermal Distortions: Core Optics, Mode Cleaner, Faraday Isolator

7.1.1.1 Core Optics, Mode Cleaner

Surface and bulk absorption in coatings and substrates of the optics lead to thermal expansion and deformation of the optic radius of curvature.[2] Absorption in coating leads to a spatially dependent surface expansion of the mirror which change the radii of curvature and modify the reflected fields in the cavity. Bulk absorption in the substrate leads to a change in the optical path variation across the Gaussian profile of the beam and a change in the effective focal length of the substrate. Small deviations in waist size (w'_0) and position Δz with respect to the nominal cavity parameters w_0 due to mode mismatch result in the introduction of the first higher order cylindrical mode V_1(r):

$$\psi(r) = \sqrt{1-\varepsilon_1^2}\, V_0(r) + \varepsilon_1 V_1(r) \qquad (2)$$

with a corresponding reduction in the coupled TEM_{00} power given by[3]

1. *Design Considerations for LIGO Mode-Matching Telescopes, LIGO-T970143-00-D*
2. W. Winkler, K. Danzmann, A. Rudiger, and R. Schilling, “Heating by optical absorption and the performance of interferometric gravitational-wave detectors,” Phys Rev A, **44**, 7022.
3. D. Anderson, “Alignment of Resonant Optical Cavities”, Appl. Opt. **23**, 2944 (1984).

$$\langle \frac{\Delta P}{P} \rangle_{Loss} = \varepsilon_1^2 = \left(\frac{w'_0}{w_0} - 1 \right)^2 + \left(\frac{\lambda \Delta z}{2\pi w_0^2} \right)^2 \quad (3)$$

Using a simplified model of absorptive surface coating and bulk heating in optical elements,[1] the change in the mirror sagitta for optical component in the COC and IOO can be computed. The results are presented in detail in *Design Considerations for LIGO Mode-Matching Telescopes, LIGO-T970143-00-D*. The resulting change in cavity mode parameters for the 4 km is shown in Table 10. By far the most serious effect is the reduction in power of the resonant sideband cavity due to the cavity instability.[1] However, since the MMT matches both the carrier and the side-bands, it is not possible to increase the sideband with the MMT without a corresponding reduction in carrier power.

Table 10: Modified TEM_{00} Cavity Parameters for the 4 km IFO

Cavity	*New Waist Size w_o' (cm)*	*Δw_o (cm)*	*New Waist Position z' (m)*	*Δz (m)*	*ε_1*
Arm Cavity (Carrier)	3.52	+0.01	969 m from ITM	-5	0.002
Recycling Michelson Cavity (Sidebands)	3.64	~0	ITM	0	0.07
Mode Cleaner Cavity	0.167	+0.001	12.25 m from curved mirror	~ 0	0.006

7.1.1.2 Faraday Isolator

The amount of mode mismatch introduced by thermal lensing (Figure 19) of the FI depends only weakly on its placement in the optical chain. Two positions are considered in order to minimize any aberrant effects. **Position 1** is between the last flat mirror of the MC and steering mirror of the MMT, ~25cm from the MC mirror. **Position 2** is between the MMT steering mirror and MMT1, ~ 37 cm from MMT1.

1. *Absorption in the Core Optics and LIGO Sensitivity, LIGO-T970xxx-00-D*

Figure 19: Thermal Lensing in the Faraday Isolator

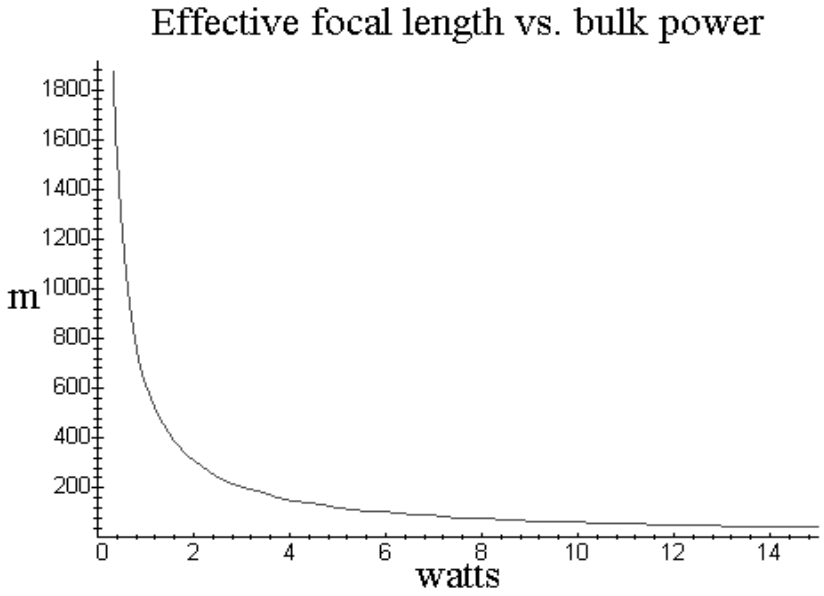

The slight shifts in mode matching are characterized in Figures 20 and 21. At 10 W, the mode mismatching and resultant power loss is shown in Table 11.

Table 11: Mode Mismatch due to thermal lensing in Faraday

Parameters	Pos. 1	Pos. 2
Δw_o *(cm)*	.178	.215
Δz *(m)*	364	284
TEM_{00} power *(%)*	99.4	98.9

Figure 20: Change in FP Arm waist position

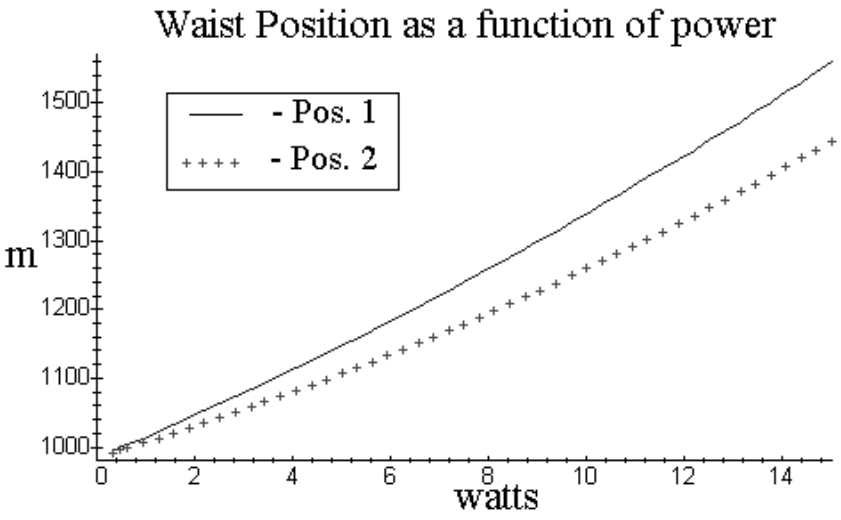

Figure 21: Change in FP Arm Waist Size

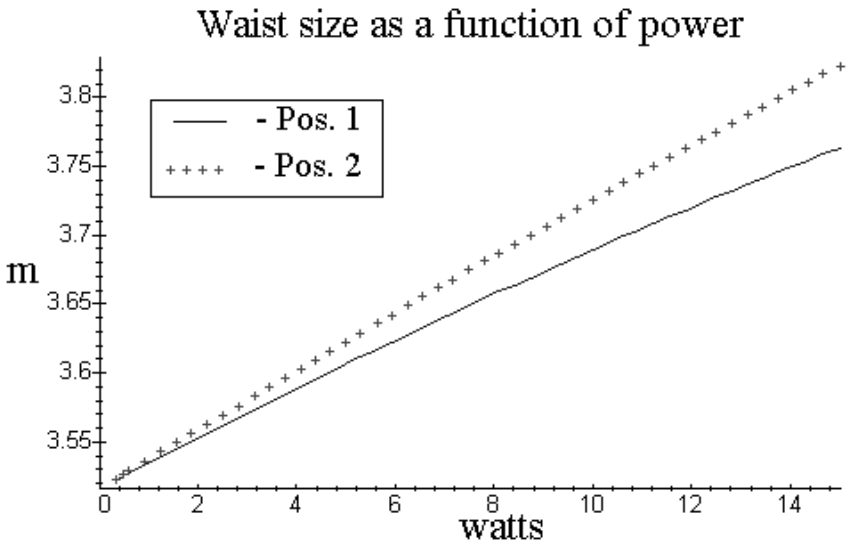

7.1.2. Surface Figure Errors in Core Optics Radii of Curvature

The LIGO interferometers utilize mirrors with large radii of curvature and correspondingly small sagitta, and are thus susceptible to errors in the nominal radii of curvature during polishing and coating. Table 12 shows the tolerances COC places on the radii of curvature errors for the core optics.[1]

Table 12: COC Curvature Error Tolerance for WA 4 km IFO

Optical Component	$\Delta R/R_{nominal}$
ETM	–0.07, + 0.01
ITM	–0.015, + 0.015
BS	TBD
RM	–0.01, + 0.05

7.1.3. Vacuum Pumpdown shifts and Stack Drift

Since the separation of the telescope mirrors will not be actively controlled, relative motions of the mirrors are expected due to shifts during vacuum pumpdown and long term thermal drifting of the vibration isolation stacks. Pump down shifts are estimated at 0.2 mm/stack.[2] SEI estimates stack drifts on the scale of 3 mm/year (translation).[3]

1. Bill Kells, “Core Optics Components Design Requirements”, LIGO-xxx
2. Mike Zucker, private communication.

7.2. Three element design

The telescope design must meet the requirements listed above, as well constraints imposed by the physical dimensions of the HAM stacks and vacuum system. In addition, we require that the telescope be able to steer the beam from the mode cleaner into the IFO, thus eliminating the need for large, flat beam steering mirrors.

The design philosophy is governed by the following criteria:

- Minimize the number of optics after the mode cleaner.
- Limit beam aperturing to the 1 ppm Gaussian intensity contour for direct path scattering
- Adjustment of the mode parameters in the IFO sufficient to meet the requirements set in Section 2.
- Minimize astigmatism introduced into the beam.
- Allow for steering of the beam into the mode IFO without significant higher order modal contamination.

These criteria lead us to select a three element telescope comprised of spherical reflective optics. Figure 22 shows the conceptual layout and definition of parameters. Table 13 lists the input parameters used in our design.

Figure 22: Definition of Parameters

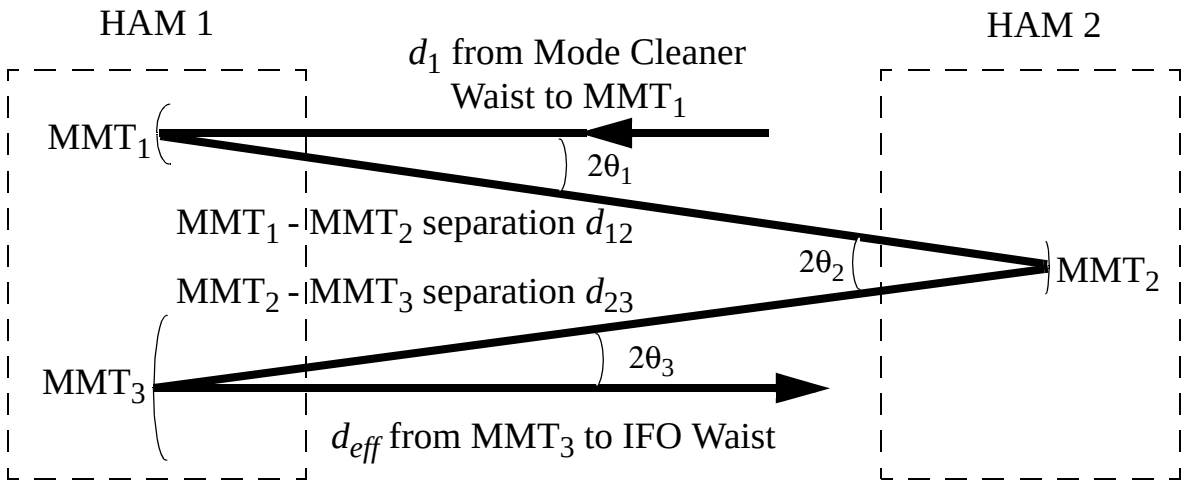

Analytical details of the design can be found in *Design Considerations for LIGO Mode-Matching Telescopes, LIGO-T970143-00-D*. Briefly, we analytically solve for *all* possible radii of curvature (R_{MMT1}, R_{MMT2}, R_{MMT3}) which mode-match to the Fabry-Perot cavity. We then use optimization to select the set which provides the *maximum* amount of adjustment of waist size and position in the core optics. The optimal values for (R_{MMT1}, R_{MMT2}, R_{MMT3}) for both the 2 km and the 4 km IFO are shown in Table 14.

3. Fred Raab, “Seismic Isolation Design Requirements”, LIGO T9600XX-X-D

Table 13: Mode Matching Parameters for the 4 and 2km IFO

	Units	4k	2k
w_0 = Waist size in Mode Cleaner	cm	0.1664	0.186
d_1 = Distance from mode cleaner waist to MMT_1	m	1.535	3.206
d_{12} = Distance from MMT_1 to MMT_2	m	13.62	13.36
d_{23} = Distance from MMT_2 to MMT_3	m	14.45	13.78
d_{rm} = Distance to recycling mirror	m	16.18	17.22
w_{eff} = Effective waist size in arms	cm	3.16	2.94
d_{eff} = Effective waist position in arms	m	1692	1161
w_3 = Waist size in arm	cm	3.51	3.15
d_3 = Waist position in arm from ITM	m	975	615.8
θ_1 = Incident angle on MMT_1	mrad	71.6	96.2
θ_2 = Incident angle on MMT_2	mrad	6.8	13.2
θ_3 = Incident angle on MMT_3	mrad	5.9	6.8
w_{m1} = Spot size on MMT_1	cm	0.169	0.195
w_{m2} = Spot size on MMT_2	cm	0.365	0.302
w_{m3} = Spot size on MMT_3	cm	3.65	3.23

Table 14: Optimal Telescope Parameters

	Δx	Δy	4 km	2 km
Optimal R_1	–	–	**9.96 m**	**11.30 m**
Optimal R_2	–	–	**2.336 m**	**2.096 m**
Optimal R_3	–	–	**26.22 m**	**25.16 m**
Maximum waist adjustment Δw_3	50 cm	~1.5 cm	0.3 cm	0.3 cm
Maximum position adjustment Δd_3	5 cm	~0.08 cm	100 m	40 m

The range of independent waist size and position adjustibility for the 4 km IFO are shown in Figures 23 and 24. The normalized TEM_{00} power coupling into the 4 km IFO as a function of the positions of MMT mirrors is shown in Figures 25-27. Two observations can be made:

- The magnitude of TEM_{00} coupled power which can be accommodated by the MMT is in the range 70%-100%

- TEM_{00} power coupling is much more sensitive to the position of mirror MMT2.

Figure 23: Independent adjustment of waist position for 4k IFO

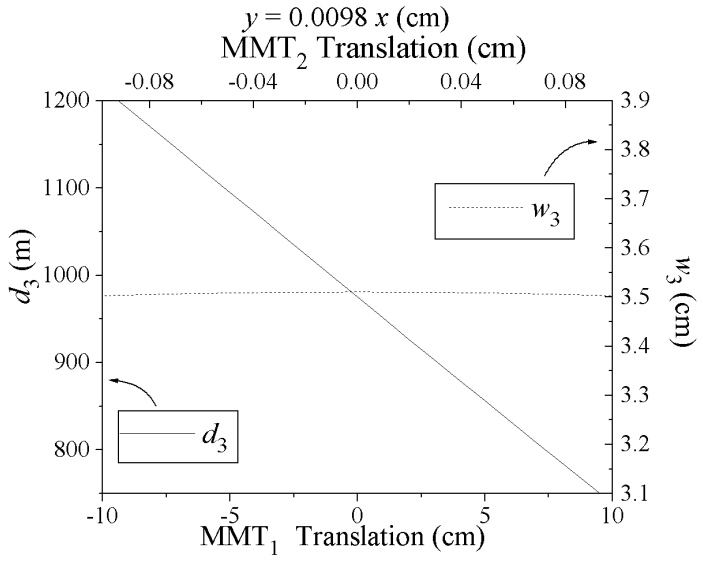

Figure 24: Independent adjustment of waist size for 4k IFO

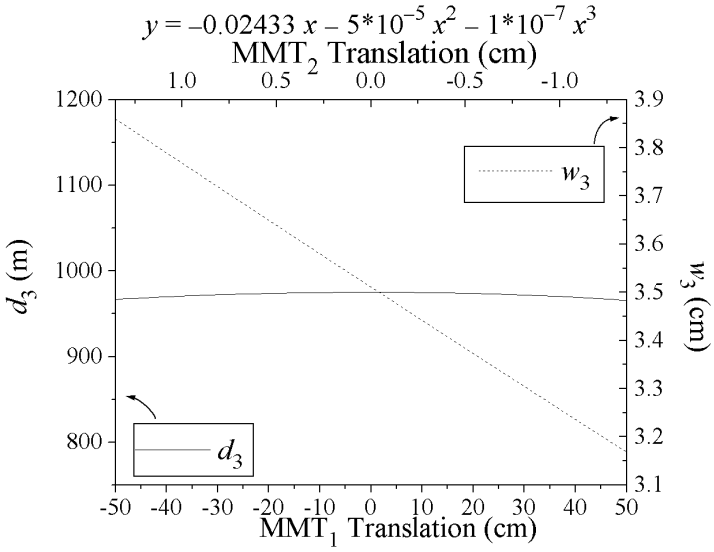

Figure 25: Power in TEM_{00} as a function of $MMT_{1,2}$ position.

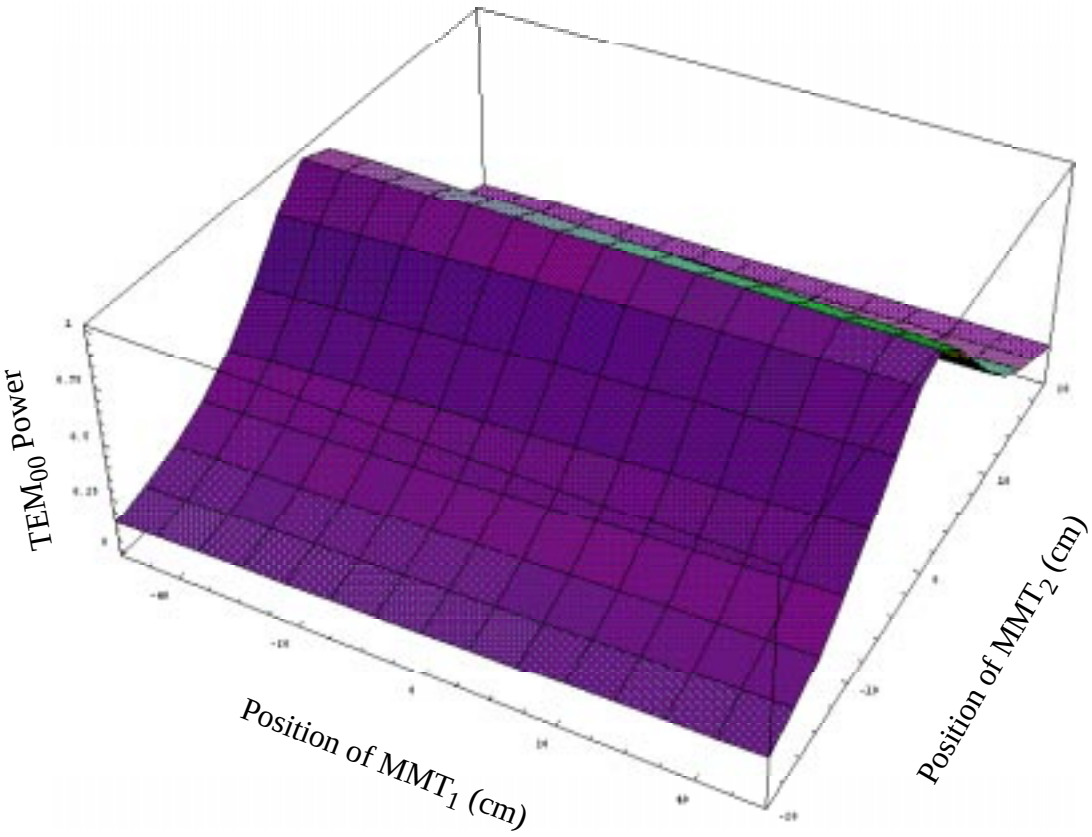

Figure 26: Power in TEM_{00} as a function of $MMT_{1,3}$ position

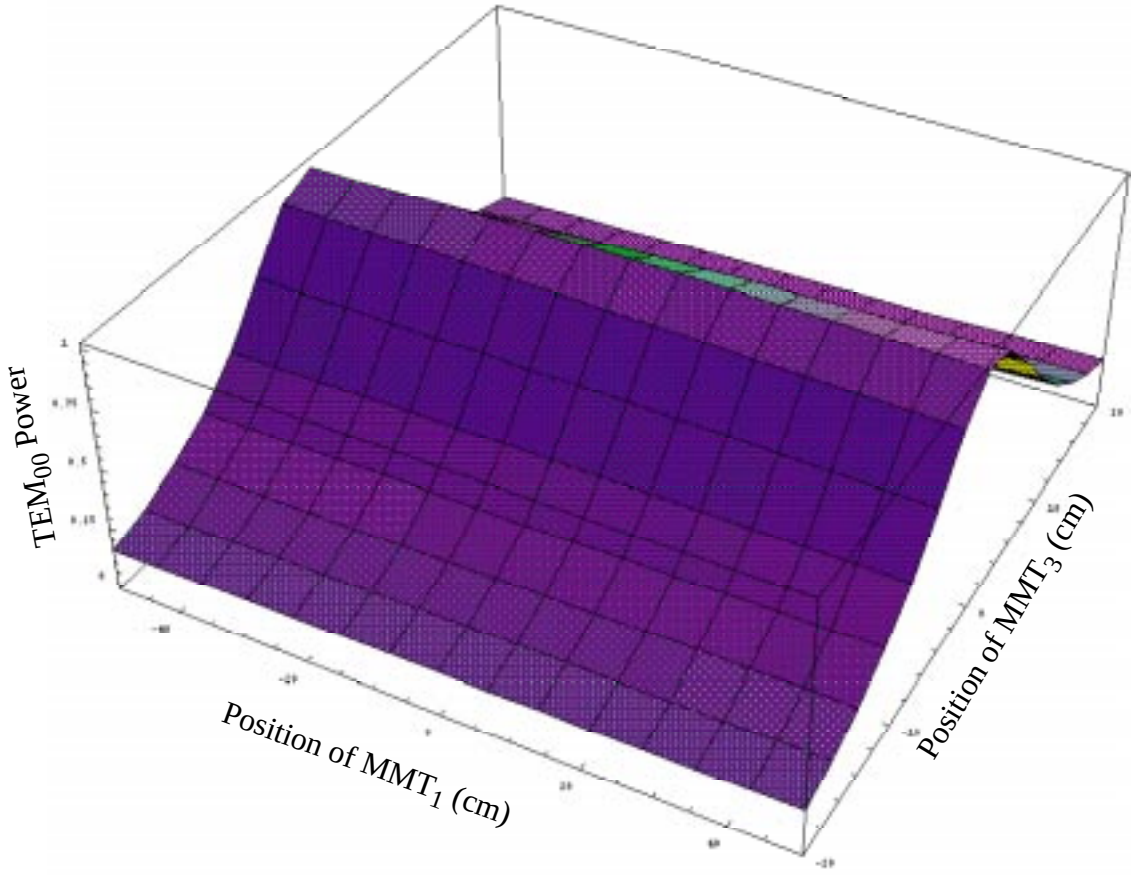

Figure 27: Power in TEM_{00} as a function of $MMT_{2,3}$ position

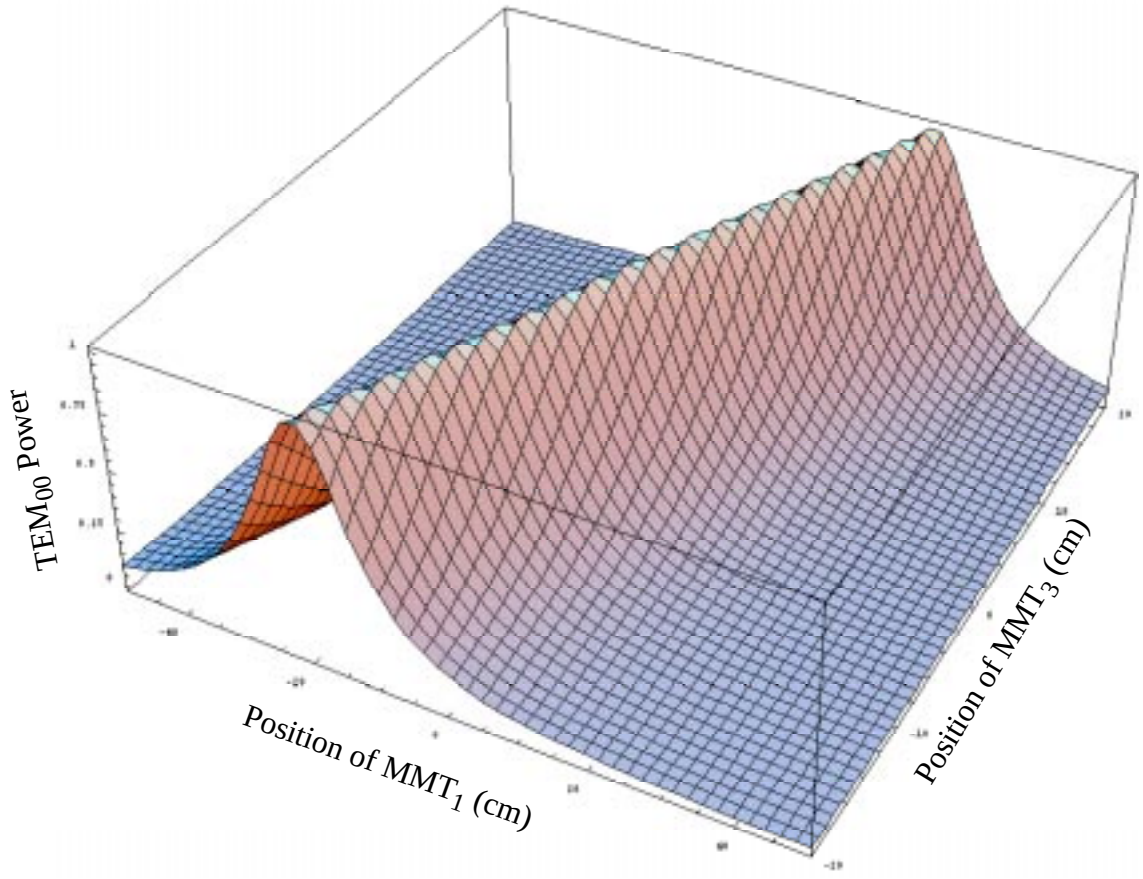

7.3. MMT Mirror Properties

7.3.1. Reflectivity and Wedge Angles

- The power reflectivity of the MMT mirrors shall be 0.999.
- The power transmission of the MMT mirrors, ~0.001, allows 10 mW to be used for MMT beam centering (see 7.7.2).
- All MMT mirrors will have 1 degree wedge angles.

7.3.2. Ghost Beams

7.3.2.1 MMT1 and MMT3

The high reflection coatings of mirrors MMT1 and 3 face toward the IFO, therefore, the amount of ghost beam power that can enter the IFO from these paths is 10^{-8} assuming 1% reflection from the back surface. Thus no baffles are needed for MMT1,3.

7.3.2.2 MMT2

The back surface of MMT2 faces the IFO. Thus, 10^{-5} of the light incident on MMT2 can directly access the IFO beam tube assuming that the beam is not blocked. The IOO will use a simple baffle located behind MMT2 and the MMT2 beam centering pick-off mirror to block the ghost beam.

7.4. Tolerances on MMT Mirror Surface Figure

7.4.1. Deviations in Radii of Curvature (Focal Error)

The tolerances for the percentage error in the radius of curvature can determined by the examining the amount of power rejected out of the TEM_{00} mode under the assumption that no compensation of mode matching occurs by moving the MMT mirrors (i.e., positioned for 100% mode-matching assuming perfect polishing) and all other optics are perfect. Our results are shown in Tables 15 and 16, which present the percentage of TEM_{00} coupled power in the FP arms for the 4 km and 2 km IFOs. It is immediately apparent that *the radii of curvature of MMT3 is the critical design parameter of the MMT.* A 0.5% deviation in the radii of curvature of MMT3 results in ~40% drop in TEM_{00} coupled power.

Table 15: Percent of Power Stored in $TEM_{0,0}$ Mode for Radius of Curvature errors on MMT mirrors for 4k

MMT_1	MMT_3	MMT_2 $\Delta R_2/R_2 = 1\%$	MMT_2 $\Delta R_2/R_2 = 0.5\%$	MMT_2 $\Delta R_2/R_2 = 0.1\%$
$\Delta R_1/R_1 = 3\%$	$\Delta R_3/R_3 = 0.5\%$	52.0	57.1	61.3
	$\Delta R_3/R_3 = 0.1\%$	89.9	94.3	97.0
	$\Delta R_3/R_3 = 0.05\%$	93.8	97.1	98.9
$\Delta R_1/R_1 = 1\%$	$\Delta R_3/R_3 = 0.5\%$	52.8	57.8	62.0
	$\Delta R_3/R_3 = 0.1\%$	90.2	94.4	97.0
	$\Delta R_3/R_3 = 0.05\%$	93.9	97.3	99.0
$\Delta R_1/R_1 = 0.5\%$	$\Delta R_3/R_3 = 0.5\%$	53.0	58.0	62.0
	$\Delta R_3/R_3 = 0.1\%$	90.2	94.4	97.1
	$\Delta R_3/R_3 = 0.05\%$	94.0	97.3	99.0

7.4.2. MMT Mirror Higher Order Astigmatic Aberrations

We have also analytically computed the loss in stored power from astigmatic figure errors ($\Delta R = R_S - R_T \neq 0$) in polishing. The change in power out of the $TEM_{0,0}$ is given for the worst possible combinations of errors (i.e. $\Delta R_1 = -\lambda/4$, $\Delta R_{2,3} = +\lambda/4$). Table 10 and 11 give a list of the

Table 16: Percent of Power Stored in $TEM_{0,0}$ Mode for Radius of Curvature errors on MMT mirrors for 2k

MMT_1	MMT_3	MMT_2 $\Delta R_2/R_2$ = 1%	MMT_2 $\Delta R_2/R_2$ = 0.5%	MMT_2 $\Delta R_2/R_2$ = 0.1%
$\Delta R_1/R_1$ = 3%	$\Delta R_3/R_3$ = 0.5%	61.9	65.7	68.7
	$\Delta R_3/R_3$ = 0.1%	92.3	95.2	97.1
	$\Delta R_3/R_3$ = 0.05%	95.1	97.4	98.8
$\Delta R_1/R_1$ = 1%	$\Delta R_3/R_3$ = 0.5%	63.2	66.9	69.9
	$\Delta R_3/R_3$ = 0.1%	92.9	95.6	97.4
	$\Delta R_3/R_3$ = 0.05%	95.5	97.7	99.0
$\Delta R_1/R_1$ = 0.5%	$\Delta R_3/R_3$ = 0.5%	63.5	67.7	70.2
	$\Delta R_3/R_3$ = 0.1%	93.0	95.7	97.4
	$\Delta R_3/R_3$ = 0.05%	95.6	97.8	99.0

percent of power that is rejected out of the $TEM_{0,0}$ mode for combinations of polishing tolerances, λ/2, λ/4, λ/10, on the three mirrors for the 4k and the 2k IFO. From this analysis, summarized in Table 17, we conclude that deviations of λ/10 are desirable and less than λ/4 are tolerable.

Table 17: Percent of Power Stored in $TEM_{0,0}$ Mode for surface figure errors resulting in astigmatic MMT mirrors for 4k IFO

	MMT_3	MMT_2 λ/2	MMT_2 λ/4	MMT_2 λ/10
MMT_1 λ/2	λ/2	95.7	96.1	96.3
	λ/4	98.6	98.8	99.0
	λ/10	99.6	99.7	99.8
MMT_1 λ/4	λ/2	95.7	96.1	96.3
	λ/4	98.6	98.8	99.0
	λ/10	99.6	99.7	99.8
MMT_1 λ/10	λ/2	95.7	96.1	96.3
	λ/4	98.6	98.8	99.0
	λ/10	99.6	99.7	99.8

7.4.3. Astigmatism Due to Off-Axis Reflection

In the steady state situation, where *x* and *y* are zero, the astigmatism can be calculated by assuming the focal length in the sagittal plane (parallel to the HAM table) is given by

$$R_{eff} = R\cos\theta \quad , \tag{4}$$

and in the tangential plane by

$$R_{eff} = \frac{R}{\cos\theta} \tag{5}$$

where θ is defined in Figure 22. Using the effective tangential and sagittal radii of curvature for each MMT, the resulting tangential and sagittal waists in the IFO can be computed. For Gaussian beams, the mode-matching coefficient is given by equation 14, and resulting reduction in fringe

Table 18: Astigmatism Introduced by 4k, 2k Telescopes

Parameter	*unit*	4k	2k
Sagittal waist, $w_{0,S}$	cm	3.512	3.161
Tangential waist, $w_{0,T}$	cm	3.508	3.142
$\lvert C_o \rvert^2$ = Percent of Power in TEM_{00}		0.9999	0.9999
Reduction in Fringe Contrast		$< 1 \times 10^{-5}$	$< 3 \times 10^{-5}$

contrast is given by $\delta F = 1 - \lvert C_o \rvert^2$. The results are shown in Table 18. From this, we conclude that spherical optics are suitable.

7.4.4. Combined Effects

In order to ensure that we have 95% power in the TEM_{00}, it is important to look at the combined effects of all calculable errors:

- surface figure errors of λ/4
- radius of curvature error of $\Delta R_1/R_1$=3%, $\Delta R_2/R_2$ = 0.5%, and $\Delta R_3/R_3$ = 0.1%
- thermal lensing in the Faraday Isolator, RM and ITM
- off axis effects
- no compensation of mode-matching by movement of MMT mirrors

Power in the TEM_{00} mode assuming RMS distribution: 96%

Power in the TEM_{00} mode assuming worst case distribution: 92.5%

- surface figure error on the MMT_3 λ/10
  - Average power in the TEM_{00} is 96.9%
  - Worst case of 94.7%
- Radius of curvature tolerance for MMT_3 to ΔR3/R3 = 0.05%

- Average power in the TEM_{00} is 98.7%
- Worst case of 97.4%

If we include compensation in power loss by adjustment of the position of the mirrors.

- Moving MMT_1 by -50 cm
- MMT_2 by -1 cm

Power in the TEM_{00} mode assuming worst case distribution with compensation: 97.5%

7.5. Optical Modeling Results

As a way of verifying and corroborating our analytical results, the optics in the IOO were modeled in ASAP™ (Breault Research) with the optical layout as specified in the ACAD mechanical drawings. Both the 4k and 2k systems were modeled and analyzed in full 3D in order to comply with the COC layout specifications.

7.5.1. Geometrical Aberration Analysis

The classical methods for Gaussian beam propagation analyze all “third-order” aberrations as perturbations to the standard paraxial theory. Among these aberrations, it is straightforward to show that petzval curvature and distortion are negligible, due to the imaging properties of the optical system. The Seidel aberrations which we must consider, however, are coma, spherical aberration, and the much scrutinized astigmatism.

Figure 28: Wavefront in Fabry-Perot Arms (4k)

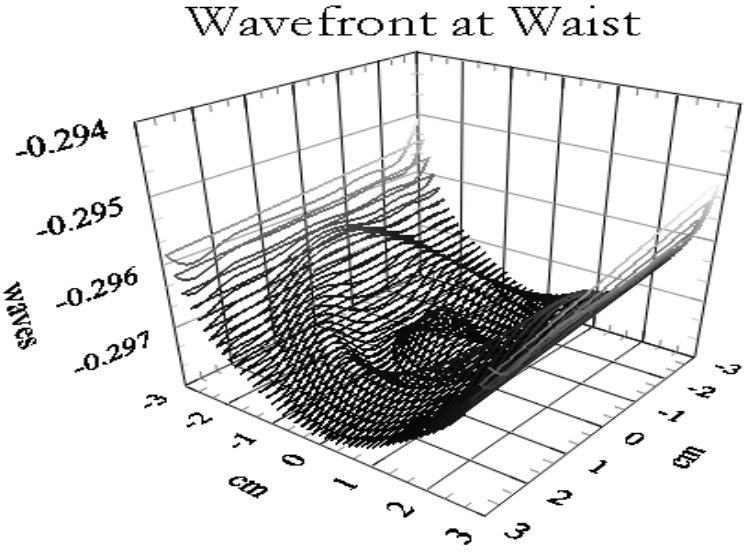

7.5.2. Wavefront Analysis

By propagating a Gaussian TEM_{00} beam of the parameters specified by the Mode Cleaner through the MMT and looking at the wavefront distortion at the cavity waist position in the

Fabry-Perot arm, one can analyze the wavefront function W(x,y) as a deviation from the ideal flat wavefront of a Gaussian beam. With perfectly smooth mirrors, all the wavefront distortion is due purely to the geometrical aberrations introduced by the use of off-axis, spherical mirrors. These results are given in Figure 28 and Table 19.

Table 19: Zernike Coefficients of Fig. 29 (nm)

	Grid Size (cm)	Z_2	Z_4	Z_6	Z_8	Z_{10}	Z_{11}	*rms*
4k	w_0	-.155	36.9	-.031	-.097	-.031	-28.5	46.6
	$2w_0$	-.888	18.3	.205	-.545	-.129	-14.4	23.3
	12.5	4.91	-12.6	-3.13	3.43	1.43	-15.8	21.3
2k	w_0	-.252	59.9	.014	-.132	-.062	-46.4	75.8
	$2w_0$	1.49	29.0	-.911	1.03	.178	-23.6	37.4
	12.5	1.05	38.9	-1.67	-.381	-.339	-2.48	39.1

7.5.3. Modal Analysis

Taking the same field and looking at the amplitude distribution A(x,y) one can expand it as a superposition of the cavity modes of the Fabry-perot arm.

$$A(x,y) = \sum_{m,n} c_{mn} u_m(x) u_n(y) \qquad (6)$$

Where $u_m(x)$ and $u_n(y)$ are the orthonormal Hermite-Gaussian eigenfunctions of the cavity. Numerically integrating each $TEM_{m,n}$ mode over the data set yields the corresponding amplitude of each mode and then directly the power. Presently, a combination of numerical errors in both the optical program and the expansion, result in an rms error on the order of 10^{-4} watts. Nevertheless, the power in the $TEM_{0,0}$ as predicted by this method is > 99.99% in the case of perfect optics, for both the 4K and 2K IFO. The 4 km result is shown in Figure 29. This shows that the current configurations of the MMT *do not contribute significantly to the coupled power loss as a result of any geometric aberrations*.

Figure 29: Field Amplitude Profile of the 4 km Beam at the Arm Cavity Waist

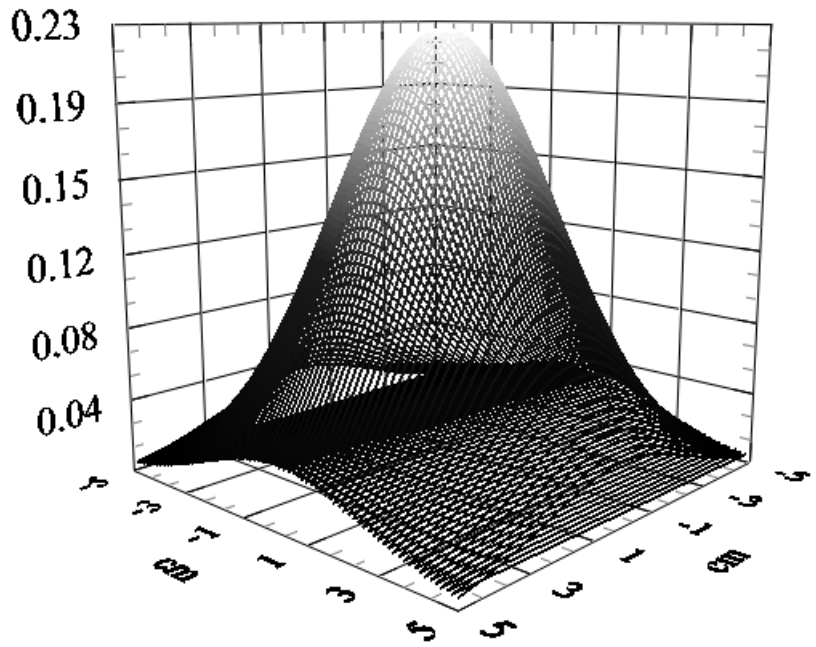

7.5.4. Surface Deformations

Rather than analyze the effects of randomly deformed optics, some research was done into discovering the typical types of deformations found on optics of the specific sizes and polishing types that are in the telescope. Three common types of surface deformations were analyzed using the methods developed above:

- Astigmatic surface on small optics
- Radially symmetric aberrations on large optics
- Errors in specified radius of curvature (ΔR/R)

7.5.4.1 Astigmatic Surfaces on $MMT_{1,2}$

The magnitude of the deformation is included within the specified surface figure error tolerances where the tolerance is Δs, the sag in each direction. Tolerances as relaxed as $\lambda/2$, do not shift more than 0.01% power out of the $TEM_{0,0}$ mode.

7.5.4.2 Radially Symmetric Aberrations on MMT_3

In general, $TEM_{0,0}$ power loss due to donut aberrations is a function of the amplitude, radius of the deformation. Writing the aberration as a function:

$$S(A, w, r) = A \cdot (\sin(wr))^{10} \quad (7)$$

where *A* is the amplitude, *w* determines the radius of the circle (spatial frequency), and *r* is the radial distance. The magnitude of the surface deformation shown in Fig. 30 is greatly exaggerated.

Figure 30: Radially Symmetric Aberration on MMT_3

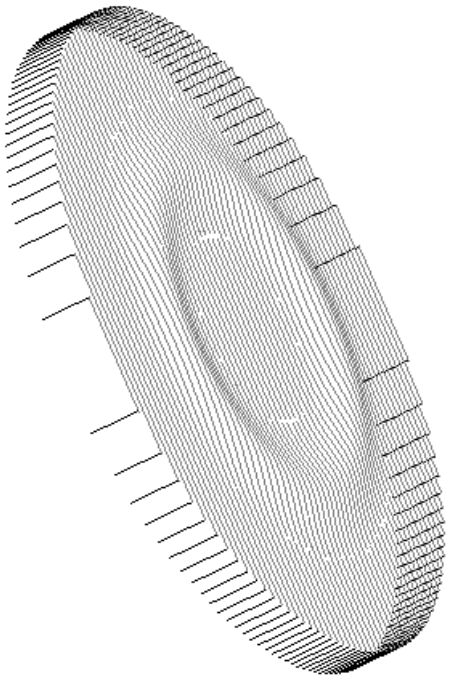

Table 20: (%) Power Loss in $TEM_{0,0}$ due to Radial Aberration

R	*A*		
	λ/10	λ/20	λ/40
w_0	83.3	83.8	91.3
$2w_0$	84.5	91.5	99.7
12.5	99.9	99.9	99.9

Table 20 shows the power losss due to these aberrations for various values of *w* and *r,* where *R* is the radius of the 'donut' shaped aberration. It should be noted, however, that ASAP modeling of these deformation for $R = w_0$ violated the paraxial approximation and, as such, may not have precision at the level of the other results. It is seen from Figure 31 that a donut aberration on MMT3 at w_0 at the level of λ/20 causes severe wavefront distortion. We thus require aberrations less than λ/40.

Figure 31: Wavefront Caused by Radially Symmetric Aberrations on MMT3

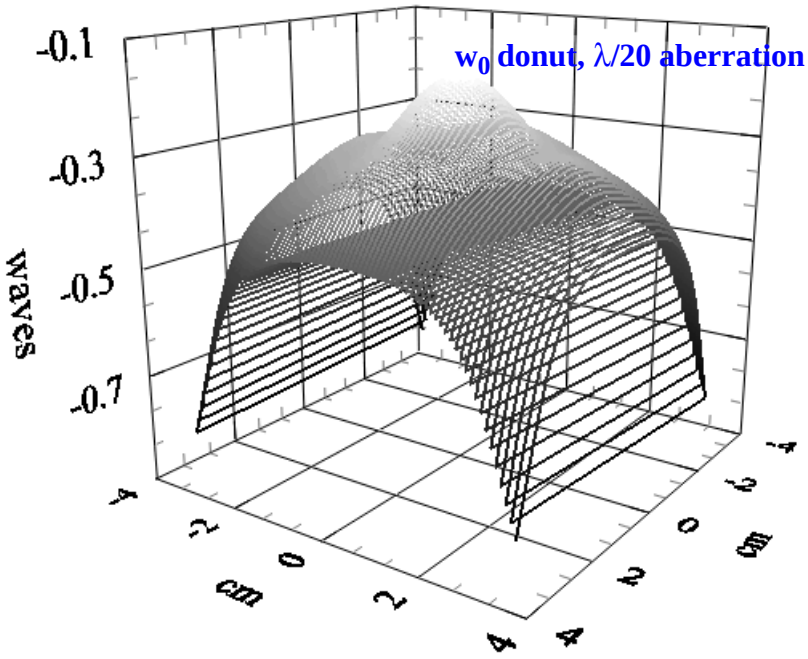

7.5.4.3 Focus Errors

Using the same methods as above, the power lost due to radius of curvature (focus) error was analyzed and was found to disagree somewhat with analytical results (see Table 21). The differences are due in part to fitting errors in recovering the Hermite-Gaussian modes and to our inability to analytically model all aberrations.

.

Table 21: Coupled $TEM_{0,0}$ Power w/ Radius of Curvature errors on MMT mirrors

IFO	MMT_1	MMT_2	MMT_3	Analytical Result (%)	Numerical Result (%)
	ΔR/R (%)				
4K	3	.5	.1	94.3	97.5
	3	1	.05	93.8	96.9
	1	.5	.05	97.3	99.4

IFO	MMT_1	MMT_2	MMT_3	Analytical Result (%)	Numerical Result (%)
	ΔR/R (%)				
2K	3	.5	.1	95.2	98.8
	3	1	.05	95.1	98.1
	1	.5	.05	97.7	99.6

7.6. Beam Steering (Mirror Misalignment) and Jitter

In order to estimate the amount of static and in-band higher order modal contamination introduced by beam steering and jitter, we use a one dimensional modal model based on the formalism of Hefetz, et al.[1] and ASAP numerical modeling. Details can be found in *Design Considerations for LIGO Mode-Matching Telescopes, LIGO-T970143-00-D.*

7.6.1. Beam Steering

For beam steering, the loss of TEM_{00} power is shown in Table 22 for the case where MMT mirrors were misaligned about the z -axis (out of the page) to determine associative power loss. It can be shown that misalignment in the other angular degree of freedom are not as serious.

Table 22: Percentage Coupled $TEM_{0,0}$ Power w/ Angular Misalignments

Misalignment (μrad)	MMT_1	MMT_2	MMT_3
+10	99.6	70.2[a]	n/a
-10	99.6	69.7	n/a
+1	> 99.9	> 99.9	71.1[a]
-1	> 99.9	> 99.9	70.0[a]
+.1	> 99.9	> 99.9	> 99.9
-.1	> 99.9	> 99.9	> 99.9

a. IFO acquisition mode required power

Coupled misalignments at 10, 1, and 0.1 μrad, respectively, yield < 1% power loss in most cases. The (-10,-1,-.1) combination yields ~3% loss.

1. Y. Hefetz, N. Mavalvala, and D. Sigg, “Principles of Calculating Alignment Signals in Complex Resonant Optical Interferometers”, LIGO T960005-00-R.

7.6.2. Beam Jitter Performance

In-band frequency noise (jitter) on the input beam into the IFO can couple to static misalignment of the IFO optics and introduce spurious in-band signals. Using the output jitter specification from the mode cleaner[1] and assuming seismic excitation of the suspensions consistent with the LA site,[2] we find that the in-band modal composition of the light is not affected by the telescope. Table 23 shows the jitter at the input to the telescope and at the input to the IFO.

Table 23: Telescope-induced Jitter

	Before Telescope	*IFO Input*
Angular Fluctuations (rad/$\sqrt{\text{Hz}}$)	6.3×10^{-13}	3×10^{-14}
Displacement Fluctuations (m/$\sqrt{\text{Hz}}$)	2.8×10^{-12}	1×10^{-10}
ε_1 (1/$\sqrt{\text{Hz}}$)	3.5×10^{-9}	3.5×10^{-9}

7.7. Alignment

7.7.1. Initial Alignment

7.7.1.1 Mirror Separation

Since the TEM_{00} coupled power is insensitive at the 0.01% level to millimeter changes in the telescope mirror separation, conventional tooling can be used for setting the initial separations of the MMTs. Removable templates for the MMT1,2 SOS and MMT3 LOS, referenced to a known position on the HAM stacks, will be used to position MMT 1,2,3 on the HAMs to within 1 mm of design positions. This will be adequate for initial separation.

Once the initial separation is set, vacuum pump down shifts of ~ 2 mm and ASC alignment of COC will require at least one iterative repositioning of the MMTs to new positions.

7.7.1.2 Angular Alignment to MC,COC

For MMT3, IOO will follow the ASC protocol for alignment.[3] A Sokkia electronic distance measurement theodolite (ASC standard measuring equipment) which has been referenced to the ETM to within 0.5 mrad will be autocollimated using an optical flat and first used to align ITM according to the procedures described in *ASC Initial Alignment.* The theodolite will then be turned 180 degrees toward MMT3. Before the RM is put in place, the angular and transverse positions of MMT3 will be set to ASC alignment tolerance and locked using an optical lever. Upon completion, the RM can be positioned and aligned.

1. J. Camp, D. Reitze, and D. Tanner, “Input Output Optics Design Requirements”, LIGO-T9600-0-D
2. G. Gonzalez, “ASC: Environmental Input to Alignment Noise”, LIGO-T960103-0-D
3. K. Mason and M. Zucker, “ASC Initial Alignment”, LIGO-T970151-00-D

Alignment of the beam from the MC into the telescope will be accomplished by using a pilot (dummy) beam (10 mW, 670 nm) which transmits through the flat mirrors of the MC to define the beam line into the telescope. (See Figure 32; We assume that the MC mirrors have been aligned to 2 x 10^{-5} rad, the MC optical axis alignment tolerance.) A thin (< 3 mm), dichroic BS (transmissive at 670 nm, reflective at 1064 nm) will be place at near normal incidence (<5 degree) in the pilot beam line to allow for a 100 mW, 1064 nm beam to be aligned and propagated collinearly to the red pilot beam. Optical targets (cross hairs) will be placed in front of the MMT optics and serve as alignment targets for the IR pilot beam aligned to the optical axis of the MC. MMT1 and 2 have small (~2-3 mm) spot radii and therefore should be accurately positioned to the center (within 1 mm) of the optic simply by cross hair alignment. MMT3 has a large (3.6 cm) field radius and therefore will require a video camera to monitor alignment to the 1 mm centering level. Once alignment is achieved, the positions of the mirrors on the MMT optics will be referenced to quad position sensors located on ISC tables beside the HAMs.

Figure 32: MMT Initial Alignment

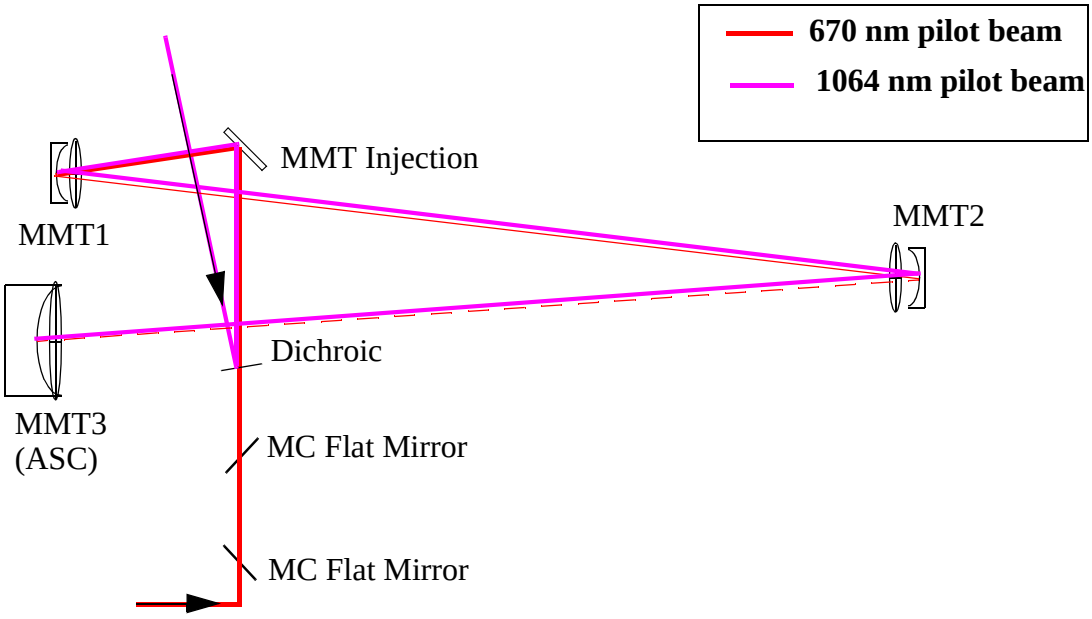

7.7.2. Alignment Control

To maintain the positions of the beam on the center of the MMT mirrors to the tolerances specified in 7.5, IOO will use a quadrant photodiode scheme as shown in Figure 33 below. 10 mW light leakage from each MMT mirror will be directed to quadrant detector located on ISC tables next to the HAM stacks. Conventional quadrant photodiodes (Hamamatsu Silicon Quadrant Photodiode; 0.3 A/W responsivity@1064 nm) located on ISC tables located next to the HAMs will be used as references for MMT beam centering.

Table 24 shows the centering requirements and corresponding angular and displacement requirements for the 4 km MMT. The centering requirements were calculated by requiring that the beam

displacement on MMT3 caused by transversely displacing or tilting MMT1 and 2 is less than the centering requirement of 1 mm on MMT2. The corresponding quadrant displacement is computed by converting the transverse displacement to angular tolerance and propagating the beam to the quad sensor. We assume a differential stack to ISC table drift of 10 µm/day.

The error signal for the MMT3, the tightest requirement, is shown in Figure 34, calculated by integrating a TEM_{00} over a split detector as a function of displacement in units waist of beam waist. A 1100 µm displacement corresponds to photocurrent error signal 5 x 10^5 over dark current noise.

Table 24: Beam Centering for 4 km MMT

Element	*Centering Requirement*	*Angular Tolerance*	*Quad PD Displacement*[a]
MMT1	1000 µm	100 µrad	5 mm
MMT2	1000 µm	437 µrad	1.25 mm
MMT3	1000 µm[b]	70 µrad	1.1 mm

a. Assumes PD is 2 m from optic
b. Assumes ASC angular control of MMT3

Figure 33: Telescope Beam Centering

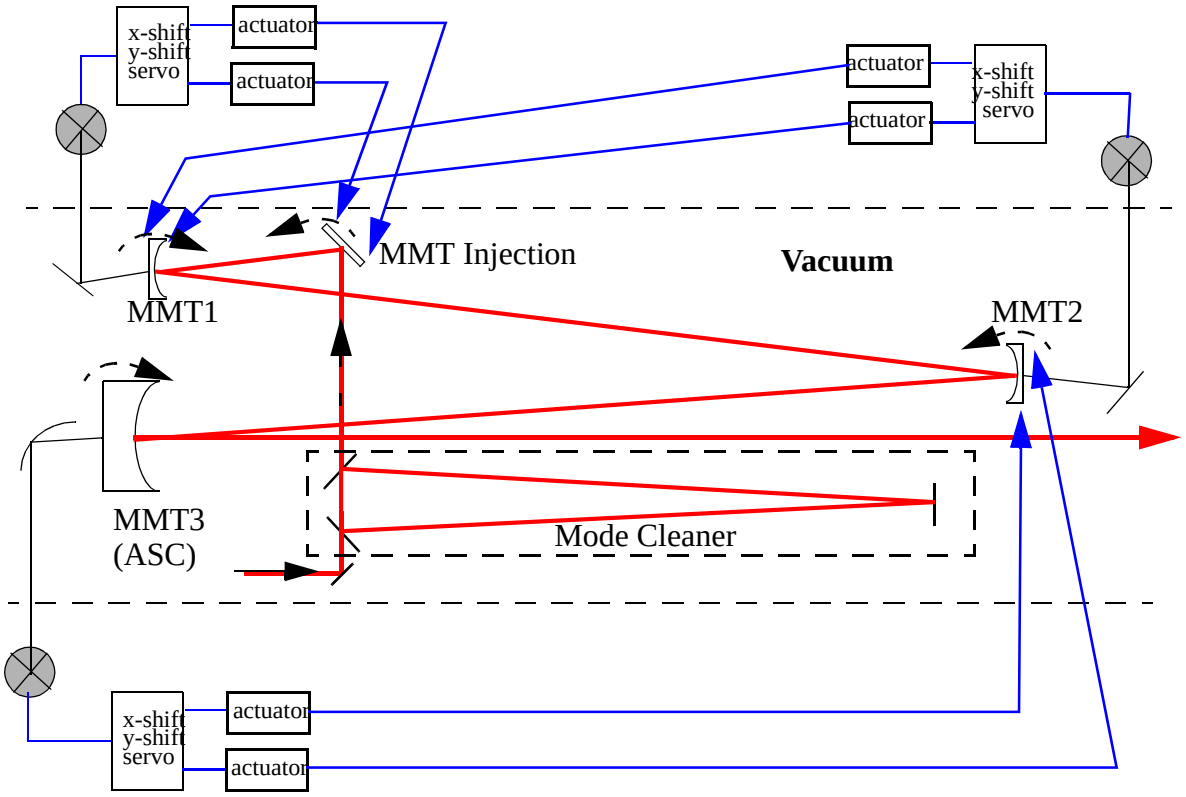

Figure 34: Error signal for De-centering of MMT2

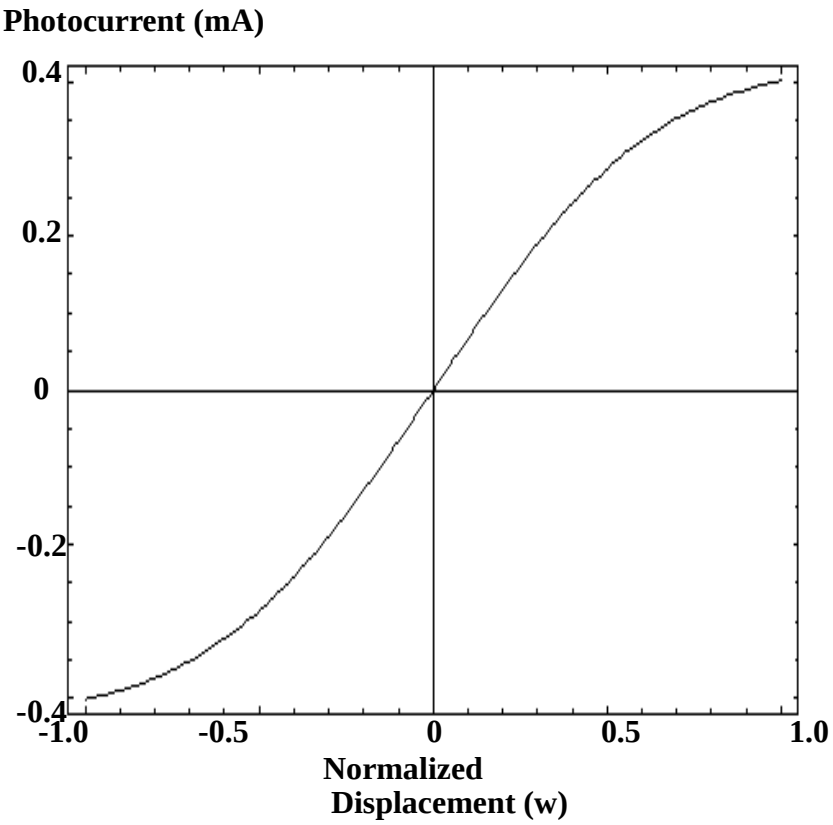

8 OPTICAL THROUGHPUT

The IOO must deliver 75% of the TEM_{00} light emerging from the PSL to the IFO, including all integrated losses from reflection, transmission, and absorption in the IOO optical components. The following table shows the transmission of the components of the IOO components. Numbers are rounded to 3 digits. For the suspended components we have assumed coatings comparable to those of the core optics, with 30 ppm loss on reflectance. The small optics are assumed to have antireflection coatings that match the Ealing narrowband multilayer coatings (0.1%). The largest individual loss comes from the large Faraday isolator, where the polarizing components contribute to a total loss of 8%. We gain considerably from the elimination of the first Faraday isolator that was in the conceptual design.

Table 25: Optical efficiency of IOO system

Item	*Loss(%)*	*Transmittance*	*Accumulated Transmittance*
RF modulation core optics	1.0	0.990	0.990
RF for mode cleaner	1.5	0.985	0.975
3 mode matching lenses	0.6	0.994	0.970
HAM1 window	0.2	0.998	0.968
3 beam steering mirrors	0.06	0.999	0.997
Mode cleaner	5	0.950	0.919
Faraday isolator	8	0.920	0.845
Mode matching telescope (4 mirrors)	0.45	0.996	0.841

9 DIAGNOSTICS

9.1. RF Modulation

The IOO will have an optical spectrum analyzer (Tropel) on the PSL/IOO table for analyzing RF side bands on the PSL table.

9.2. Mode Cleaner

Since we are not actively controlling the sideband frequency relative to the mode cleaner length, an RF photodiode will be used to periodically monitor the amount of excess noise induced by a laser frequency dither coupled to a frequency detune of the MC. RF frequency and/or MC length adjustments will be made manually when necessary. See Section 6.4, Mode Cleaner Length Controls.

The IOO will have the capability to monitor MC cavity ring down times using a fast photodiode on located on the ISC table.

9.3. IFO Mode-Matching Telescope

9.3.1. Measurement of Mode-Matched Power

Measurement of mode matched power will utilize two donut position sensors[1] to measure the mismatch of cavity waist size and position. Figure 35 shows a diagram of the measurement, in which the mismatch is measured using the back-reflected light from the RM.

9.3.1.1 Expected performance

- A 100 μm offset of MMT3 (limited by SOS dynamic range) results in a change in ε_2 amplitude (first higher order cylindrical mode) of ~ 10^{-3}.
- SOS force imbalance (~ 1%) between magnets results in an unwanted angular misalignment of ~ 10 μrad for MMT2. The angular misalignment gives a contribution for the TEM_1 mode ε_1 approaching unity.
- ASC loop gains at 0.1 Hz are ~100, thus attenuating the ε_1 mode and yielding $\varepsilon_2/\varepsilon_1$ ~1.
- The annular shape of the PD gives an additional factor of 100 CMRR for the $\varepsilon_1$mode assuming the optimal Guoy phase,[1] giving more than adequate signal of 10:1 for the donut WFS.

1. *Modal Model Update 4: Mode-Matching, LIGO-T960116-00-D*

Figure 35: WFS Measurement of the Mode Mismatch

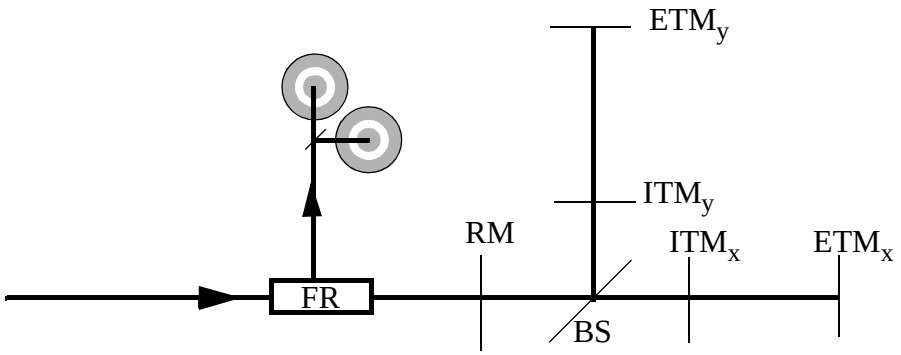

9.3.1.2 Prototype Implementation

In order to verify the performance of the donut WFS, the IOO group will develop a prototype donut WFS using a small (20 cm) reference cavity. A (partial) survey of photodiode vendors has revealed that annular geometries are not off-the-shelf items. While we continue to look for split-annular PD vendors, we intend to simulate a split detector with two, masked single PDs. For a 20 cm cavity with a two element telescope, an analysis similar to the one above (assuming a 10 μm dither, angular misalignment of 10 μrad, and CMRR of ~100 yields an expected $\varepsilon_2/\varepsilon_1$ signal ~10:1.

10 TEST AND PROCUREMENT PLAN

10.1. IFO Mode Matching Telescope

Our modeling results indicate that RC_{MMT3}, the radii of curvature of the third telescope mirror, is the most sensitive design parameter of the telescope design, with a 0.5% change in R_{MMT3} resulting in a drop in TEM_{00} power to ~65% in both IFOs. We contacted two polishing houses, General Optics (G-O) and Argus International, to survey the achievable polishing precision for MMT3 (25 cm diameter, 10 cm thick fused silica substrate, RC=26.22 m):

- **Vendor: General Optics**
  - super-polish
  - $\Delta R/R$ (focus error) < 0.4%
  - higher order aberrations < $\lambda/10$ at 632 nm
  - Cost/optic: $5,000.00 (substrate not included)

- **Vendor: Argus International**
  - super-polish
  - $\Delta R/R$ (focus error) < 0.05%
  - higher order aberrations < $\lambda/10$ at 632 nm
  - Cost/optic: $1,950.00 (substrate not included)

Substrate vendors (Corning, Heraeus) have been contacted but have not yet responded to RFQs.

The variance in $\Delta R/R$ specifications of almost a factor of 10 lead us to adopt the more conservative specification of ~ 0.4% as an achievable number. Given the sensitivity of MMT3, we propose to work around this tolerance limitation by implementing the telescope design in three stages:

10.1.1. Procurement of MMT3

Using the baseline design above, an order will be placed for MMT3 specifying the tolerance to 0.4%. The lead time for procurement is ~ 6 months.

10.1.2. Measurement of MMT3 Radii of Curvature

Upon receipt of the optic, the radii of curvature will be measured to a level of 0.2%. The sag of a 25 cm, 25 m radii of curvature optic is ~ 300 μm. This corresponds to ~ 500 fringes on a Fizeau interferometer using He-Ne light and therefore should be easily achievable.

10.1.3. Redesign of MMT1,2

Once the radii of curvature of MMT3 has been characterized to the 0.2% level, the radii of MMT1,2 will be recomputed to optimize the baseline mode-matching with the new RC_{MMT3}, since MMT1,2 are not as sensitive to changes in radii of curvature. This will produce a final MMT design in which MMT1,2 are matched to MMT3.

10.2. High Power Effects

Transmissive optical components in the beamline will be subjected to 8 - 10 W average powers over prolonged durations. Exposure to sustained power levels can cause adverse effects on beam quality which in turn will degrade the LIGO strain sensitivity.

10.2.1. Requirements

10.2.1.1 Thermal Lensing

Caused by uniform low level absorption which can change the output modal parameters of the beam (spot size, radius of curvature).

- Requirements:
  - Must maintain 95% power in TEM_{00} mode in IFO
  - Focus error (Z_2) must be compensated by IFO MMT.

10.2.1.2 Non-uniform Beam Spatial Variations

Caused by local microscopic absorption regions and spatial variations in the index of refraction which can change the shape and output pointing of the beam (modal contamination).

- Requirements:
  - Must maintain 95% power in TEM_{00} mode in IFO.

10.2.1.3 Polarization contamination (elliptization)

Caused by thermally-induced birefringence.

- Requirements:
  - Static: maintain polarization purity at 100:1 level (CHECK)
  - Dynamic: polarization fluctuation --> AM

$$\theta_{pol} < 10^{-4} \text{ rad}/\sqrt{\text{Hz}} \text{ to maintain } 10^{-8} \text{ PSL stabilization}$$

10.2.2. Laser Source and Characterization Equipment

A Lightwave multi-frequency, 10 W, 1.064 micron laser will be adequate for performing these tests. (Longitudinal modes of the laser are in the GHz regime and therefore will not interfere with RF noise characterization.)

10.2.2.1 Beam/Modal Quality

Beam quality will be assessed by transmitting a known modal structure (Gaussian parameters) through the optic in question and measuring the output mode as a function of intensity in excess of LIGO level intensities. Deviations in beam quality and modal parameters will be measured using a commercial beam profiling system (Wavefront Sciences) capable of measuring changes in mode parameters at the $\lambda/120$ level

- Measurements
  - Short term characterization of modal changes

- Long term (> 1 week) sustained exposure at high intensity

Figure 36: Thermal Lensing Measurement

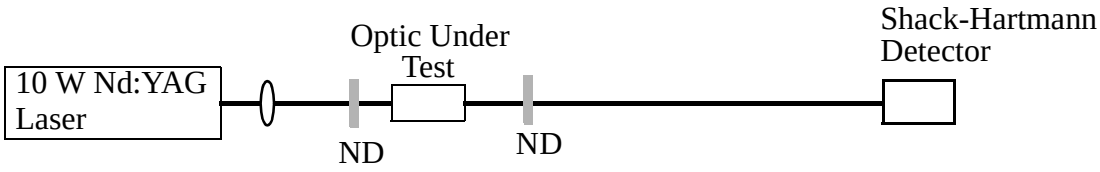

10.2.2.2 Beam Pointing

Beam jitter occurring at in band frequencies degrades the shot noise limited sensitivity of LSC and ASC. Thermally induced beam pointing jitter will be measured using a quadrant (position sensitive) photodiode placed in the far field of the beam. (See Figure 36.) The output of the diode will be sent to a spectrum analyzer and measured as a function of intensity.

Figure 37: Beam Jitter Measurement

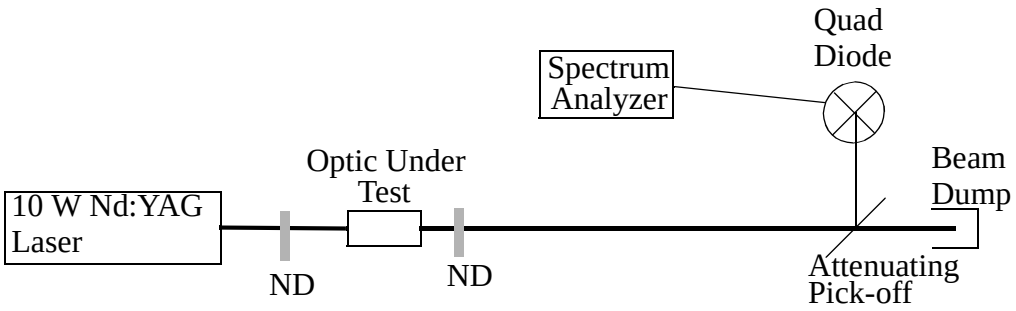

10.2.2.3 Beam Polarization

Intensity dependent measurements of beam polarization will be made by picking off a small portion of the beam analyzing the polarization using a Glan laser polarizer, and RFPD, and a spectrum analyzer.

Figure 38: Polarization Measurement

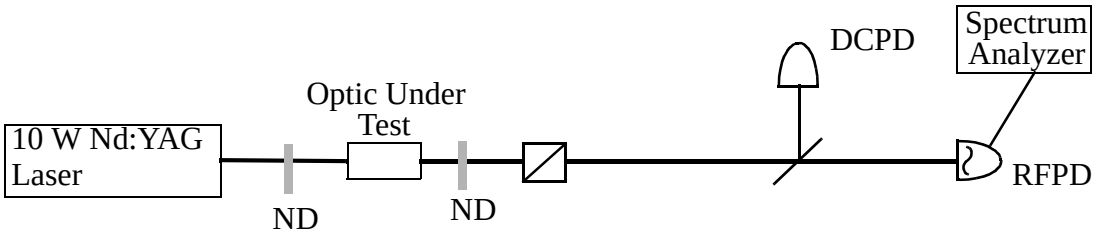

10.2.3. Specialized EOM, Faraday Isolator Testing

Specific testing of for the EOM and FI will also take place.

10.2.3.1 EOM

Modulation characteristics (modulation index and amplitude modulation) may have some laser power dependence. Tests will be performed to measure the modulation index and amplitude modulation by measuring the RFAM with an RF photodiode and signal spectrum analyzer and the sideband height will be measured with an optical spectrum analyzer.

Figure 39: EOM Testing

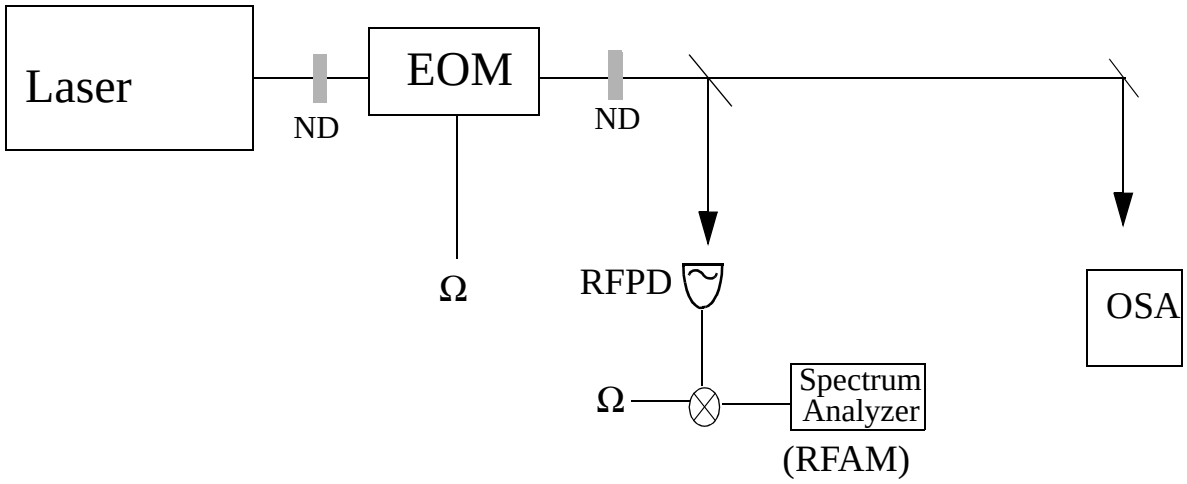

10.2.3.2 Faraday Isolator

The power dependence of the isolation of the Faraday isolator will be determined by back-reflecting the light into the FI, measuring the rejected light with a power meter and the non-rejected light with a photodiode (the ratio should be constant for power-independent isolation).

Figure 40: FI Isolation Testing

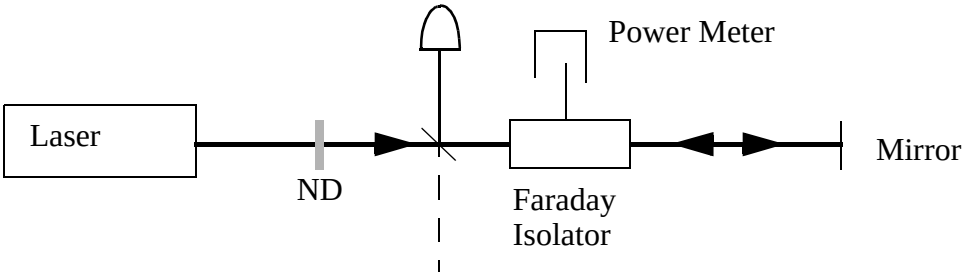

APPENDIX 1

Beam wiggle

Assumptions -

- The incident beam is originally TEM_{00}
- Wiggle of the incident beam is represented by higher order Gaussian modes

Effect on the higher order-suppression formula -

Consider Figure 14 where M_1 is the input mirror and M_3 is the output mirror. We consider two cases: case 1 in which the incident beam is introduced into the mode cleaner in such a way that it goes through the shorter arm first and case 2 in which it goes through the longer arm first.

Figure 41: Triangular mode cleaner

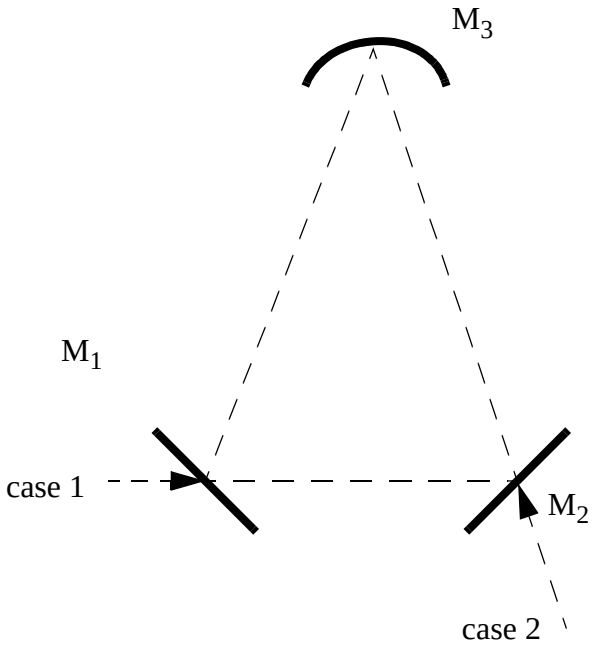

In the first case the incident beam encounters M_1, M_2, M_3, M_1, M_2,... in this order. After one triangular trip the output beam from M_2 is

$$A_1 = t_1 r_2 r_3 r_1 t_2 e^{2i\delta}$$

where the phase is measured relative to the phase if the mode cleaner is removed. This continues for the second and further trips, giving the equation for the Fabry-Perot resonator.

$$t = \frac{t_1 t_2}{1 - r_1 r_2 r_3 e^{2i\delta}}$$

Next, consider case2. This case differs from case 1 only in the order in which the incident beam goes through the mirrors. Therefore, mathematically, if the subscripts 1, 2 and 3 for r and t in the above equations are replaced, the same formulas can be used. Because all of the above formulas are symmetric with respect to the order of r_j and t_j, j=1, 2, 3,...., the resultant formula representing the fraction of the high order power transmitted through the resonator is insensitive to such replacements. This means that whether the incident beam is introduced as case 1 or 2 does not affect the wiggle suppression efficiency of the mode cleaner, provided that the same higher order modes are generated by wiggle.

Does the difference in the introduction of incident beam generate different higher order modes for a given wiggle?

Now the question is whether case 1 and case 2 generate the same higher order modes for a given incident misalignment. To discuss this, consider the mode cleaner as an equivalent periodic lens system.

Figure 42: Equivalent lens system

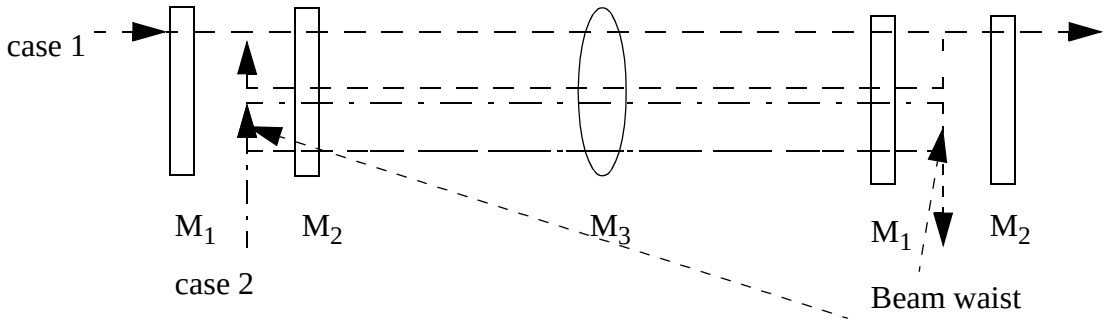

The incident beams for the two cases can be treated as shown in Figure 15. Thus the only optical path difference between the two cases is the path between M_1 and M_2 that case 1 experiences in the first and last trips. From the second trip through the final trip, there is no optical path difference. In either case, the whole optical system is arranged in such a way that a beam waist is formed in the middle of the space between M_1 and M_2. This means that the distance from this beam waist to the original beam waist formed by the laser cavity must be the same for the two cases. Therefore, any wiggle taking place upstream to M_2 should result in the same deviation in the mode cleaner from the originally designed ray geometry (in the radius of curvature, beam direction, etc.), generating the same higher order modes.

From what is discussed above, it is clear that the difference in the mode cleaner mirror to introduce the incident beam does not affect the wiggle suppression capability of the mode cleaner.